REPUBLIC OF TÜRKİYE

ALTINBAŞ UNIVERSITY

Institute of Graduate Studies

Electrical and Computer Engineering

BACKSCATTER-ASSISTED NON-ORTHOGONAL MULTIPLE ACCESS FOR ULTRA-MASSIVE MACHINE-TYPE COMMUNICATIONS IN 6G NETWORKS

Mustafa Adnan Abed ABED

Doctor of Philosophy

Supervisor

Prof. Dr. Osman Nuri UÇAN

İstanbul, 2026

BACKSCATTER-ASSISTED NON-ORTHOGONAL MULTIPLE ACCESS FOR ULTRA-MASSIVE MACHINE-TYPE COMMUNICATIONS IN 6G NETWORKS

Mustafa Adnan Abed ABED

Electrical and Computer Engineering

Doctor of Philosophy

ALTINBAŞ UNIVERSITY

2026

The dissertation titled BACKSCATTER- ASSISTED NON-OR THOGONAL MUTLIPLE ACCESS FOR ULTRA- MASSIVE MACHINE TYPE COMUNICATIONS 6G NETWORKS prepared by MUSTAFA ADNAN ABED ABED and submitted on 07/01/2026 has been **accepted unanimously** for the degree of PhD in Electrical and Computer Engineering.

____

Prof. Dr. Osman Nuri UÇAN

Supervisor

Thesis Defense Committee Members:

Prof. Dr. Osman Nuri UÇAN	Department of Electrical-Electronic Engineering, Altınbaş University	_______________
Assoc.Prof. Dr. Sefer KURNAZ	Department of Computer Engineering, Altınbaş University	_______________
Assoc. Prof. Dr. Abdullahi Abdu IBRAHIM	Department of Software Engineering, Altınbaş University	_______________
Asst. Prof. Dr. Serdar KARGIN	Department of Biomedical Engineering, İstanbul Arel University	_______________
Prof. Dr. Adil Deniz DURU	Department of Sports and Health Sciences Marmara University	_______________

I hereby declare that this dissertation meets all format and submission requirements for a PhD thesis.

I hereby declare that all information/data presented in this graduation project has been obtained in full accordance with academic rules and ethical conduct. I also declare all unoriginal materials and conclusions have been cited in the text and all references mentioned in the Reference List have been cited in the text, and vice versa as required by the abovementioned rules and conduct.

Mustafa Adnan Abed ABED

Signature

ABSTRACT

BACKSCATTER-ASSISTED NON-ORTHOGONAL MULTIPLE ACCESS FOR ULTRA-MASSIVE MACHINE-TYPE COMMUNICATIONS IN 6G NETWORKS

ABED, Mustafa Adnan Abed,

Ph.s., Electrical and Computer Engineering, Altınbaş University

Supervisor: Prof. Dr. Osman Nuri UÇAN

Date: 01/2026

Pages: 82

6G cellular networks will require to provide significantly higher system capacity and user data rates. This potential growth along with today's shortage of spectrum increases the need for new frequency spectrum. The new millimeter wave spectrum is emerging as a suitable candidate with a large amount of available bandwidth (around 60 GHz). The new spectrum places a new requirement for single element antenna and array design. This work addresses the issues of mm-wave antenna design and the problems that designer may face during the designing process. The proposed antenna has a resonating frequency of 26 GHz and 2 GHz bandwidth. Beam squint problem is also analysis in this work. The results showed that the gain of the mm-wave antenna array becomes a function of frequency which significantly reduces the performance of mm-wave communication system. Millimeter wave (mmWave) wireless technology has become a part of human life for high-speed and secure data transmission. A square microstrip patch antenna with a resonance frequency of 26GHz was proposed in this work for mmWave wireless communication. One square radiating element makes up the antenna. CST Microwave Studio, an electromagnetic simulation program, was used to construct and study the suggested antenna on a Rogers RO 3003 lossy substrate with a relative permittivity of 3. This work's outcome demonstrates a minimal return loss of -19.34 dB, a gain of 6.97 dBi, and a bandwidth of 2GHz at a resonant frequency of 26 GHz. The element is transformed into an 8-element uniform linear array; the suggested array boosts the gain to 16dBi while maintaining a high radiation efficiency. A high-gain wide-band planar antenna with a reconfigurable intelligent surface (RIS) is presented in this study for use in contemporary wireless communication applications. The antenna is composed of

two primary components: a basic antenna component with two light-dependent resistor switches and cross-line slots, and a second component that uses the RIS layer for beam steering. The RIS is made up of two-sided, five-by-five-unit cells that form a square. The antenna substrate is a 1.6 mm thick dielectric layer of FR4 epoxy glass. In order to attain the appropriate electromagnetic properties at the frequency band of interest, the RIS inclusions are developed and numerically tested. The manufactured prototype achieves an antenna gain ranging from 10.5dBi to 16.8dBi and exhibits a wide band covering frequencies from 0.9GHz to 3.5GHz with S11 below -10dB. Effective aperture utilization is demonstrated by experimental measurements in all shapes, and beam steering from +22° to -22° is achieved without lowering side-lobe levels. To assess channel performance in terms of bit error rate (BER) and channel capacity (CC), the suggested antenna's performance is compared to actual measurements. In contrast to traditional RIS-assisted antennae that depend on PIN or varactor switches, the presented work conducted LDR-controlled design offers compact beam steering with little insertion loss.

Keywords: Beam Forming, Steering Directions, Microstrip Circuitry, RIS, CP, Antenna, BER.

TABLE OF CONTENTS

Pages

ABSTRACT .... **V**

LIST OF TABLES .... **X**

LIST OF FIGURES .... **XI**

1. INTRODUCTION **1**

1.1 NOMA COMMUNICATIONS IN 6G 2

1.2 BSC CONCEPTS 3

1.3 LIMITATIONS 4

1.4 SIGNIFICANCE 5

1.5 RESEARCH QUESTIONS AND GAPS CLARIFICATIONS 7

1.6 PROBLEM STATEMENT 8

1.7 THESIS ORGANIZATION 9

2. THEORY AND CONCEPTES **10**

2.1 ADIEPTIVE AND STRONG PERAFOMANCE 11

2.2 AI/ML-BASED BEAMFORMING APPROACHES 12

2.3 COMPARISON OF ADVANTAGES AND LIMITATIONS 13

2.4 BEAMFORMING IN 5G AND EMERGING 6G SYSTEMS 14

2.4.1 Massive Mimo and Its Impact on Spectral Efficiency 14

2.4.2 Millimeter-Wave and Terahertz Beamforming 15

2.4.3 6G Innovation Keys 15

2.5 SPECTRAL EFFICIENCY IN WIRELESS NETWORKS 16
2.6 CHALLENGES 17
2.6.1 Hardware Limitations 17
2.6.2 Channel Estimation Errors 18
2.6.3 Trade-offs between Beamforming Complexity 19
2.7 RELATED WORK AND COMPARATIVE ANALYSIS 20
2.8 SUMMARY OF LITERATURE REVIEW 20
3. RIS SYSTEMATIC DESIGN 28
3.1 METHODOLOGY AND DETAILS 29
3.2 IRS DESIGN GEOMETRICAL DETAILS 32
3.2.1 Single Element 32
3.2.2 Array Shape 34
3.3 PERFORMANCE STUDY 35
3.3.1 Single IRS Results 35
3.3.2 Array Results 37
4. DESIGN AND EVALUATION 40
4.1 ANTENNA DESIGN AND GEOMETRICAL DETAILS 42
4.2 DESIGN METHODOLOGY 43
4.2.1 Antenna Performance without RIS Inclusions 44
4.2.2 RIS Design 47
4.2.3 RIS Effects 50
4.3 EXPERIMENTAL REALIZATIONS AND MEASUREMENTS 53

4.3.1 Antenna Validation Performance 54

4.4 PERFORMANCE CHANNEL 58

5. CONCLERUSION AND FUETURE WORCKS 60

5.1 CONCLERUSION 60

5.2 FUTURE WORK 61

REFERENCES 63

LIST OF TABLES

Pages

Table 2.1: Critical Observations and the Need for Proposed Research.............................. 23

Table 3.1: Geometrical Parameters of the Antenna... 34

Table 4.1: A Comoparason Betwean the Prroposed Study and Othar Published Results... 59

LIST OF FIGURES

Pages

Figure 3.1: Methodology and Details. 31

Figure 3.2: IRS Layer Based on Array Shape from CST MWS.. 32

Figure 3.3: Unit Cell Design from CST MWS: (a) Front View and (b) Back View........... 33

Figure 3.4: The Result of IRS Array Based on the Proposed Unit Cell from CST MWS. . 35

Figure 3.5: S11 Curve of Single Element from CSTMWS. 36

Figure 3.6: Farfield Pattern 2D at f=26 from CST MWS... 36

Figure 3.7: Gain Variation over Frequencies from CST MWS... 37

Figure 3.8: Antenna Array Farfield at f=26 GHz from CST MWS. 37

Figure 3.9: The Evaluated Antenna Performance Based on S11 and Gain Spectra from CST MWS.. 38

Figure 3.10: Attenuation Using 5G Prediction Models from CST MWS For (A) Lower Operating Frequency of 26Ghz (B) Higher Operating Frequency of 28.5Ghz. 39

Figure 4.1: Shape of the Proposed Antenna: (A) 3D Viaew, (B) Antena Petch Viaew, (C) RIS Froent Viaew, and (D) RIS Back Viaew. 43

Figure 4.2: The Coneidared Caeses. 45

Figure 4.3: Simulated Reseaults of the Antena With out RIS Layer: (A) S11 Spectra, (B) Polarization Spectrumes, and (C) Gain Spectrumes.. 46

Figure 4.4: The proposaed Unitsell of the Proposead RIS: (A) Unitsell detaeiles and (B) Waveaguide Anaelyses. 47

Figure 4.5: The Evelueted S-Peramaters of the Proposead RIS Unitcell: (A) Eveluataed S11 and (B) S12. 49

Figure 4.6: The Evaluated S-Parameters of the Proposed RIS Unit Cell with Different Switching Shapes: (A) Evaluated S11 and (B) S12. 50

Figure 4.7: Simulated Results of the Antenna with RIS Layer: (A) S11 Spectra, (B) Polarization Spectra, and (C) Gain Spectra. 51

Figure 4.8: The Evaluated Antenna Radiation Patterns Based on the RIS Layer with Different Shape Process: (A) E-Plane and (B) H-Plane. 53

Figure 4.9: The Fabricated Antenna Prototype: (A) The Considered Antenna Patch, (B) The Antenna Structure, And (C) The Proposed RIS. 54

Figure 4.10: Antenna Veliadation Reseults: (A) S11 Speactrum and (B) Radaition Patterns at 0.915Ghz At Different Switching Shapes. (B.1) The Antenna Radiation Patterns at 00_Shape, (B.2) The Antenna Radiation Patterns At 01_Shape, and (B.3) The Antenna Radiation Patterns at 10_Shape. 56

Figure 4.11: Measured Antenna Radiation Patterns at 0.915GHz At Different Polarization and Orientation: (A) E-Plane and (B) H-Plane... 57

Figure 4.12: The Evealuated Pereforamance in Tearms of: (a) BER and (b) CC. 58

ABBREVIATIONS

3GPP	:	Third Generation Partnership Project
5G	:	Fifth Generation
6G	:	Sixth Generation
AI	:	Artificial Intelligence
ANN	:	Artificial Neural Network
AoA	:	Angle of Arrival
AoD	:	Angle of Departure
AP	:	Access Point
AWGN	:	Additive White Gaussian Noise
BER	:	Bit Error Rate
BF	:	Beamforming
BS	:	Base Station
CCDF	:	Complementary Cumulative Distribution Function
CNN	:	Convolutional Neural Network
CSI	:	Channel State Information
DL	:	Deep Learning
DoA	:	Direction of Arrival
DNN	:	Deep Neural Network
DoF	:	Degree of Freedom
EIRP	:	Effective Isotropic Radiated Power
EM	:	Electromagnetic
EVM	:	Error Vector Magnitude
FDD	:	Frequency Division Duplex
FFT	:	Fast Fourier Transform
GA	:	Genetic Algorithm
GPU	:	Graphics Processing Unit
IoT	:	Internet of Things

IRS	:	Intelligent Reflecting Surface
LoS	:	Line of Sight
MIMO	:	Multiple Input Multiple Output
ML	:	Machine Learning
mmWave	:	Millimeter Wave
MRC	:	Maximal Ratio Combining
NLoS	:	Non-Line of Sight
OFDM	:	Orthogonal Frequency Division Multiplexing
QoS	:	Quality of Service
RIS	:	Reconfigurable Intelligent Surface
RF	:	Radio Frequency
RL	:	Reinforcement Learning
RNN	:	Recurrent Neural Network
RSSI	:	Received Signal Strength Indicator
SDMA	:	Space Division Multiple Access
SE	:	Spectral Efficiency
SINR	:	Signal-to-Interference-plus-Noise Ratio
SNR	:	Signal-to-Noise Ratio
TDD	:	Time Division Duplex
UE	:	User Equipment
UL	:	Uplink
URLLC	:	Ultra-Reliable Low-Latency Communication
UAV	:	Unmanned Aerial Vehicle
V2X	:	Vehicle-to-Everything
ZF	:	Zero Forcing

LIST OF SYMBOLS

ω	:	Angular Frequency
α	:	Attenuation Constant
C	:	Capacitive
γ	:	Complex Propagation Constant
σ	:	Conductivity
J	:	Current Density
dB	:	Decibel
p	:	EBG Unit Cell Width
E	:	Electric Field Intensity
W_1	:	Patch’s Substrate Width
L_1	:	Patch’s Substrate Length
W_2	:	Patch Width
L_2	:	Patch Length
W_3	:	Unit Cell Width
L_3	:	Unit cell Length
W_4	:	Feeding Width
L_4	:	Feeding Length
W_5	:	Aperture Slot Width
L_5	:	Aperture Slot Length
W_6	:	Feeding’s Substrate Width
L_6	:	Feeding’s Substrate Length
λ_g	:	Guided Wavelength
θ	:	Incident Angle
L	:	Inductive

H	:	Magnetic Field Intensity
LFSS	:	FSS Length
WFSS	:	FSS Width
W_1	:	Patch Width
μ_o	:	Permeability of Free Space ($4\pi\times 10^{-7}$ H/m)
ε_o	:	Permittivity of Free Space (8.85×10^{-12} F/m)
β	:	Phase Constant
Γ	:	Reflection Coefficient
L_f	:	Reflector length
C_r	:	Reflector Length (Downside)
C_f	:	Reflector Length (Top side)
W_r	:	Reflector Width-Down
μ_r	:	Relative Permeability
ε_r	:	Relative Permittivity
f_r	:	Resonant Frequency
c	:	Speed of Light in Free Space (3×10^{8} m/s)
d	:	Thickness Substrate of the Proposed Antenna
T	:	Transmission Coefficient

1. INTRODUCTION

Communications are undergoing transformative evolutions that extend beyond the Fourth and Fifth Generations (4G and 5G). Notably, the Sixth Generation (6G) is being envisioned. The promising 6G uplink signals must conserve energy and completely satisfy the exponential growth of emerging services in the ultra-Massive Machine-Type Communications (umMTC) paradigm. Various design dimensions (connectivity, coverage, capability, security, sustainability, system architecture, etc.) must comply with 6G design parameters. umMTC seeks to realize a high-connected Network-of-Things (NoT). Fundamental communication frameworks also need development, even developments of orthogonal transmission concepts such as NOMA and hybrid Active/Passive NOMA (AP-NOMA), since conventional approaches either perform inadequately or generate high-user interference. The 6G vision must satisfactorily fulfil multi-faceted bona fide traffic demands while conserving energy [1] and spectrum through efficient (NOMA) cooperation.

Backscatter Communication (BSC) technology is proposed to overcome the umMTC challenge at the transmitter side. Devices employ backscatter techniques that exploit the existing RF carriers for both energy harvesting and information transfer. NOMA assistance is being integrated into backscatter-assisted communications due to convergence with massive low-rate umMTC demands and the complementary recovery of wireless spectrum and energy supply. NOMA passively integrates the backscatter channel into the active channel and affected users/packets transmit concurrently by associating different resource parameters. However, the integration of BSC-NOMA lacks coverage of optimum resource allocation and power control for AP-NOMA.

The continuous evolution from 4G to 5G, and the following journey toward 6G networks, is driven by a fundamental change in telecommunications. Fourth-generation networks focus on high-speed mobile broadband with sufficient coverage, mainly for enhanced mobile broadband (eMBB) applications, such as high-definition videos and virtual reality.

In contrast, five-generation mobile systems concentrate on three new service categories: URLLC, eMBB, and mMTC. In this stage, new technologies like NOMA and backscatter broadcasts are developed to meet the needs of future wireless networks [1]. The main goal of 6G networks is to enable ultra-umMTC over a large area, with at least 107 devices/km^2.

In very busy places like factories and subway stations, users only send short data packets (2–32 bytes) every hour, but they need coverage that can reach up to 1 km. The biggest problems are energy, connection, and spectrum. After green communications come ultra-massive machine-type communications.

Consequently, simultaneous-wireless-information and power-transfer (SWIPT) becomes a generally employed approach, enabling low-power and non-rechargeable battery-free devices to harvest energy from radio frequency (RF) signals before data transmission. These networks significantly enhance spectral and energy efficiency while alleviating interference [2]. However, the widespread adoption of massive machine-type communications induces severe spectrum scarcity, thereby resorting to hybrid active-passive backscatter communication or backscatter-assisted NOMA technologies [3].

1.1 NOMA COMMUNICATIONS IN 6G

The sixth generation of wireless networks, or 6G, is envisioned to address the urgent challenges and unmet needs that remain for the communication systems of the fifth generation (5G) and, in particular, to extend and enhance the ability to communicate within and beyond the scope of traditional human-to-human (H2H) connectivity. Support for ubiquitous ultra-massive machine-type communications (umMTC), in which a network must handle a huge number of devices exchanging sporadic small amounts of data while simultaneously catering to H2H demands, is a key element in this regard.

Such a system must operate at very low average power. Meanwhile, spectrum availability is becoming more constrained; existing bands may be shared only under particular conditions, and new allocations require significant regulatory effort. Consequently, 6G must retain and enhance the ability to support low power and long-range connections. Hybrid active-passive BSC and NOMA transmit and manage information in fundamentally different ways and may therefore be viewed as complementary techniques.

Backscatter-assisted NOMA (BAC-NOMA) provides simultaneous-energy and spectrum-cooperation between the up-link and down-link. Existing hybrid schemes consider only either BSC or NOMA as an active technology or focus on multicarrier systems. Further, merely applying backscatter to an existing NOMA design may offer performance inferior to that of even active orthogonal multiple access systems. A unified BAC-NOMA framework that incorporates BSC resource allocation, cooperation requirements, power-domain interference management, and energy harvesting could therefore advance umMTC beyond the present state of the art [1] [6] [7].

1.2 BSC CONCEPTS

BSC is a cutting-edge technique that uses very little energy to enable devices in passive mode to connect with an access point (AP). A radio frequency (RF) signal that was previously sent by the access point (AP) is reflected by the backscatter device in the BSC. This makes it possible for the BSC to send its own data. Backscatter-assisted non-orthogonal multiple access (BAC-NOMA) communication allows backscatter devices (BDs) and active users (AUs) to share the same spectrum from the access point (AP) simultaneously. In this way, backscatter devices can use the same spectrum as active users. Ultra-massive multi-machine communication (umMTC) applications greatly benefit from this BSC and NOMA combination [1]. Since NOMA technology allows numerous users to share a physical layer, it will be necessary for future cellular networks. Its growing popularity is due to its ability to meet the needs of ultra-massive multi-machine communication (UMMTC), a technology required for the deployment of networks beyond 5G and 6G [1]. The power domain multiplexing technology allows numerous users to access the same time-frequency resource at the same time. NOMA users with different channel conditions might be multiplexed during uplink transmission because users with less-than-ideal channel conditions might need more transmit power to attain the same level of quality of service (QoS) [8].

This feature is essential for umMTC because of the devices' constrained power supply. However, energy-sustainable umMTC also requires a downlink transmission scheme that can satisfy extensive energy harvesting and reduce the shortening of battery life. Owing to its simultaneous energy and information transmission feature, backscatter communication (BackCom) is a promising candidate. In addition, BackCom enables passive transmission without using any active RF front-end, which saves battery power and extends the lifetime of the devices. Nevertheless, one BackCom device may only transmit to one active device at the same time.

As a result, the potential of integrating NOMA with BackCom to construct a BackCom-assisted NOMA (BAC-NOMA) system arises. The uplink and downlink transmissions in

BAC-NOMA can be simultaneously and continuously operated without any time-frequency switch and dedicated resource allocation at the device side. The uplink and downlink transmissions can also cooperatively and jointly proceed due to the low-pass characteristic of the BackCom channel.

1.3 LIMITATIONS

NOMA has emerged as a pragmatic solution to accommodate the demands of 6G ultra-massive machine-type communications (umMTC) by allowing tandem transmission to multiple users on the same resource. Although hybrid backscatter-assisted NOMA schemes extend umMTC capabilities further facilitating energy harvesting and spectrum-efficient connectivity first-generation NOMA remains insufficient on its own to deliver the scalability, sustainability, and coexistence critical for ubiquitous, ultra-massive connections [1].

NOMA is a good way to build future 6G networks because it lets multiple users share the same time or frequency resource. With orthogonal multiple access (OMA), each user gets their own channel resources. With NOMA, multiple terminals can talk to each other at the same time using power-domain or code-domain multiplexing. NOMA lets more terminals be scheduled at the same time than OMA can handle in ultra-massive machine-type communications. But these methods still put too many limits on how much energy can be used. They let more than 100,000 devices connect while staying within the strict energy budget set by ultra-massive applications [8]. A good way to get around these problems is to use backscatter communications with NOMA.

It makes sure that ultra-massive communications will work well even when there isn't much bandwidth and there is a lot of path loss and co-channel interference. The emergence of Internet-of-Things (IoT) in the next-generation (NG) communication systems has raised the demand for wireless technologies due to the anticipated connectivity of billions of devices. However, the existing modern networks will need to evolve to satisfy diverse application requirements. The general features of the umMTC technology will be a key enabler of 6G networks.

To expand the IoT network without requiring excessive additional resource consumption, sustainable transmission technology is essential. Massive connectivity of battery-free low-cost sensor devices is required to ensure high-volume data collection with minimum interference [9]. Unfortunately, ubiquitous deployment of low-cost, low-power devices using traditional communications is infeasible due to the violation of energy, interference, channel-accessibility, and complexity resource constraints.

NOMA and BSC have been proposed as two promising technologies to realize sustainable umMTC for 6G networks [10]. NOMA allows simultaneous transmissions from multiple devices by utilizing the power domain to increase network capacity, while BSC is a low-cost two-way transmission technology that can lower signal transmission; simultaneously, NOMA can be integrated into BSC systems to maximize the number of users participating in umMTC within limited resources [11]. The joint usage of BSC and NOMA promotes the sustainable and secure shape of umMTC by eliminating wiring and endorsing low-cost implementation to conceivably support future 6G development.

1.4 SIGNIFICANCE

Backscatter-assisted non-orthogonal multiple access (BAC-NOMA) tackles the considerable demands of ultra-massive machine-type communications (UM-MTC) in sixth-generation (6G) networks. UM-MTC envisions an unprecedented number of ultra-reliable, ultra-low-complexity, and energy-constrained devices communicating simultaneously under the resource constraints provided by uncoordinated access. Conventional NOMA approaches enable the simultaneous transmission of information to multiple active devices by utilizing either successive interference cancellation (SIC) or power-domain NA [12].

Stationary devices or devices with very low-energy budgets can harvest energy from either ambient sources or from the transmission of either active devices or backscatter transmission. With the adoption of backscatter communication (BSC), two network operation modes (i.e., uplink and downlink) can be combined in the same time-frequency resource [1]. As long as information signal can be efficiently extracted from the backscattered signal, optimal channel estimation and block synchronization are not required. Backscatter-enabled signal is often overlapped in time with sample snooping protocols and/or lot sampling intensive [11], making the joint operation- and epoch-synchronization less demanding.

Machine-type communications (MTCs) enable devices such as sensors, actuators, and low-power Internet-of-Things (IoT)/machine-type terminal equipment to communicate without human intervention and with minimal end-user interaction. While MTC addresses IoT requirements via conventional cellular networks, ultra-massive MTC (um-MTC) demands the connection of up to 106 devices per square kilometer, raising spectrum shortage and energy-consumption concerns in conventional 4G services. Consequently, 5G and beyond are developing a spectrum-efficient and energy-conserving paradigm to support the um-MTC of 6G. The key rationale for um-MTC in the 6G vision is to monitor physical conditions at a fine-grained level using a huge number of low-cost sensors and terminal devices to collect enormous amounts of information.

Such a data-collection process has a low bit-rate requirement, allowing the evolution of MTC from Packet Data Services (PDS) and Continuous Data Services (CDS) to um-MTC—ultra-MTC with frequent report collection within time intervals. Um-MTC must support critically low device-cost, communication-range, and energy-expenditure requirements alongside energy-autonomous and connection-dense features. Backscatter communication (BSC) meets these requirements without complementary orthogonal multiple access (OMA), while NOMA copes with point-to-multipoint scenarios requiring single-user access.

An integrated BSC-NOMA (BAC-NOMA) framework consequently combines both techniques, but views BSC as conventional instead of backscatter-aided. Such frameworks remain unstudied in practical uplink/downlink um-MTC scenarios, alongside transmission-performance analysis without considering practical factors. Two central research objectives thus arise: 1) devise a BAC-NOMA resource-allocation algorithm to maximize uplink throughput amid BSC from downlink users; and 2) analyze the performance of BSC-augmented transmission under Rayleigh/Rician fading from an uplink perspective [1] and [2].

Machine-type communications (MTCs), with diverse connectivity for devices without human intervention, is a key enabler for sixth-generation networks. Ultra-massive MTCs (umMTCs) can accommodate a large number of devices and meet stringent energy requirements. Backscatter communication (BSC), which leverages ambient radio waves to transmit information without active transmission, and NOMA, which superposes multiple users' information in the power domain, are promising solutions.

Both BSC and NOMA facilitate simultaneous energy harvesting and information transmission, making them suitable for umMTC. However, existing works tend to consider BSC and NOMA separately, underutilizing their potential synergy. The State of the Art presents the existing applications of BSC and NOMA individually and in hybrid active-passive systems, motivating the study of backscatter-assisted NOMA for umMTC.

1.5 RESEARCH QUESTIONS AND GAPS CLARIFICATIONS

umMTC will serve monitoring and control applications with diverse connectivity, energy, and latency requirements, facilitating interconnection of tens of billions of IoT devices [1]. Backscatter communication (BSC) interfaces passive devices with an active wireless network by reflecting and modulating signals: radio frequency energy harvesting and ultra-low-cost operation extend battery life and enable scavenging indefinitely. NOMA tiered power-domain multiplexing with joint interference treatment enhances throughput and signing range, addressing umMTC limitations [9].

These two paradigms are thus complementary, yet separately apply only to strictly active, purely passive, or hybrid schemes and neither achieves sustainable umMTC without further integration. Simultaneous wireless information and power transfer (SWIPT) allows users to harvest energy while communicating, thus enhancing sustainable connectivity. Power-constrained umMTC in 6G systems pose formidable challenges, and NOMA and backscatter communication appear as candidates to address them.

The two paradigms are complementary: continuous energy harvesting (EH) and information decoding can only be realized with backscattering-enabled NOMA, and NOMA can impose a strict time division between active transmissions and backscattering, preserving essential H2H communication. Despite their respective strengths, a compelling gap remains: whether the integration of NOMA with backscatter communication is beneficial for umMTC purposes [1].

Hybrid active-passive systems have been separately studied, but neither passive-only nor active-only operation can guarantee sustainable connectivity. Pure backscatter and exclusively active NOMA modes fail to achieve trade-offs between throughput, EH, and interference control. System-level approaches that unify NOMA and BSC have yet to be considered for umMTC. The transmitted data of active users subject to interference depends on the target signal and represents an essential coupling that ties jointly active-backscatter communication from independent time-division schemes, ruling out conventional channel coding the fundamental principle of hybrid communication [13].

A BSC-assisted NOMA paradigm fuses backscatter transmission into the uplink of a downlink NOMA scheme, enabling simultaneous EH and information transfer, a distinct energy-water-like signal representation of active users, and flexible user division. The transmission-energy-time signals of active downlink users can be backscattered through time-division multiple access, retaining single-channel information and extending theoretical results on feasible um-MTC pairing by separating aerial-humanoid-humanoid connections from channels with sufficient aerial-uh connectivity. Three exploitation objectives uplink-throughput maximization, transmission-EH enhancement, and interference mitigation yield an array of additional insights.

1.6 PROBLEM STATEMENT

The 6th Generation (6G) systems are expected to revolutionize wireless communications by providing improved Performance Indicators enabling novel applications such as ultra-massive Machine Type Communication (umMTC). Backscatter communications (BackCom) and NOMA techniques being considered as building blocks of 6G systems can enhance umMTC. Backscatter-assisted NOMA (BAC-NOMA) allows for joint transmission using the same spectrum and time resources between the Downlink (DL) and Uplink (UL), enabling simultaneous energy and information transfer from the Downlink whilst MTDs transmit information in the Uplink.

Nevertheless, existing research has mainly focused on either backscatter communication systems or NOMA-based systems, and no theoretical framework that unifies backscatter communications with NOMA has been proposed. This work formulates a theoretical framework for backscatter-assisted NOMA in 6G Ultra-Massive MTC (UM-MTC) and conducts extensive literature review on multi user backscatter communications and backscatter communication combined with active transmission whose performance comprehensive comparison is provided against classical OMA, pure NOMA, pure BackCom using energy harvesting, Rayleigh and Rician fading channels.

1.7 THESIS ORGANIZATION

The thesis is organized as chapter 2: Literature review and theoretical background, in chapter 3: System model and analytical framework, in chapter 4: Simulation results and performance evaluation, and the thesis is finalized in chapter 5: Conclusion, contributions, and future work.

2. THEORY AND CONCEPTES

Beamforming constitutes a key technique for enhancing signal strength at target locations by employing multi-antenna arrays that create directional radiation patterns. Analog beamforming relies on phase shifters to adjust phases at each antenna element, thereby increasing gain and compensating for path loss; both active and passive phase shifters are employed, each presenting trade-offs in power consumption and area [1]. Digital beamforming is more flexible because it can change signals at the baseband level. But it doesn't work as well at higher frequencies because it needs more hardware and power. Hybrid beamforming uses precoding in both the baseband and radio-frequency (RF) phases to fix this problem. It uses phase shifters, switches, or lenses to combine the usefulness of hardware with the ability to change it. Adaptive and long-lasting beamforming techniques improve system performance and lifetime when propagation conditions are adverse [2]. Recent developments in AL: ML, DL, and NN, have made systems more flexible over time, which has improved their performance compared to traditional model-based methods. Massive MIMO system based modern communication technology enhances wireless networks beyond 5G by enabling control of each antenna element and facilitating beamforming [3]. Beamforming is a way to change the phase and strength of signals sent from multiple antennae to send the signal in a certain direction. This kind of technology is the best way to use the available frequencies. Adding more antennae makes the beams narrower, which stops people from getting in each other's way. By sending a radiation pattern to a specific location, beamforming creates destructive interference in some directions and constructive interference in others. A phased array with three antennae was used to show the idea in 1905. Because the constraints aren't convex, hybrid beamforming design needs to optimize both analog and digital precoders at the same time or separately [4]. The sparse topology of the channel at millimeter-wave frequencies in densely populated urban areas enables the application of straightforward precoding techniques that approximate optimal performance. Despite significant advancements in the field, selecting the appropriate beamforming structure remains challenging. The 5G New Radio (NR) standard says that structures below 6 GHz must be completely digital. At millimeter-wave frequencies, though, analog and hybrid systems are still preferred because they are cheaper and easier to set up. Analog beamforming can only make one beam at a time, so the base station has to quickly move the beam to serve more than one user.

The beam management techniques for 5G NR show that this is a need. In LTE, there are three main types of techniques that have been standardized for multiantenna data transmission: diversity, beamforming, and spatial multiplexing. Different transmission modes change how precoding and CSI acquisition are done, which turns on these techniques. Space-frequency coding is the basis for transmit diversity, which works by taking advantage of the fact that there are many physical antenna ports.

2.1 ADIEPTIVE AND STRONG PERAFOMANCE

The status of the channel is a critical factor in designing a beamforming technique. The technique used in aligning beams considers where the device is in order to make full use of the spectrum available. Advantages and disadvantages exist in using the spatial information in making alignments in step one of beam alignment. Changes in environments not accounted for in the early anticipations include an update in geographical information when early assumptions prove incorrect. Real-world measurement sets establish the fact that existing solutions such as old methods or methods based on subspaces do not address adequately a non-perfect and non-current dataset.

Some work has suggested using temporal correlations between the antenna domain and the physical domain in order to calculate possible future positions and achieve a balance between performance and resilience in an optimal manner. This calls for analysis and mathematical calculation in carrying out a formulation, especially in case of large arrays. [5]. Improved ML and ML algorithms assist in improving spectral efficiency by addressing issues in aligning beams in order to address interference, blockages, and context awareness. Location, pointing, and speed provide us with high-level information, which in turn assists in aligning these beams. Environment-aware deep learning algorithms to detect the most suitable settings for one and multiple base stations in order to achieve better beamforming. This enhances the signal, minimizes interference, prevents blocking, and maximizes spectral efficiency and user coverage. The system-level analysis of the millimeter wave in extended urban macro environments focuses on a comparison of contextual and non-contextual beamforming schemes relative to performance under positioning errors in different network densities and overlapping states [2].

2.2 AI/ML-BASED BEAMFORMING APPROACHES

Beamforming sends signals from antennae to specific communication links to increase capacity and reduce interference. To direct the beam, analog beamforming uses one RF chain and phase shifters. This makes it easy to use and low-power, but it can't handle more than one stream at a time. Each antenna has its own RF chain thanks to digital beamforming, which allows it to deliver multiple streams simultaneously and optimize spectrum utilization. It is more expensive and more difficult, though.

By combining the greatest features of both analog and digital systems, hybrid beamforming can address the issues associated with both. Because adaptive beamforming continuously modifies the weights for automatic spatial filtering, it can eliminate noise more effectively than previous optimization techniques. However, robust beamforming continues to function even in the event that the guiding vectors are not the same. Beamforming chooses the best beam pattern and precisely guides it using AI and ML. It works well in environments that are subject to fluctuations. Because of its versatility, it is especially helpful in situations where preserving signal clarity is essential, such as radar systems and telecommunications. Engineers can improve performance and guarantee dependable communication in a variety of scenarios by utilizing these cutting-edge technologies. 6G development is being driven by the need to make greater use of the spectrum. Spatial diversity is one way that massive MIMO might boost capacity. With bandwidths ranging from many gigahertz, this tendency is particularly evident in the terahertz and millimeter-wave bands. Reconfigurable intelligent surfaces (RIS) use reflections to expand coverage, and extra spatial flexibility is provided by umMIMO with more than 256 components. Massive MIMO in 5G can function with both high- and low-antenna correlations to help achieve ultra-massive MIMO goals. To maximize the benefits of the 6G communication system, we need to devise ways to enhance the spectrum [2]. The result is the quantity of information that can be sent over a given bandwidth, which is commonly known as spectral efficiency (bit/s/Hz). It has an instant impact on how quickly data transactions may be transmitted and received over a network. For 6G networks to operate effectively, precise channel status data, low beam interference, and perfect beam alignment are necessary. Techniques such as precoding, cooperative beamforming, and multi-user scheduling can be used to improve spectral efficiency. These strategies work well for minimizing interference and optimizing resources. Improvements in software and hardware solutions that can adjust to changing network conditions will also be necessary to achieve optimal spectrum efficiency. Additionally, by using AI for real-time decision-making, the network's ability to dynamically manage resources will be enhanced, further enhancing overall performance. Hardware limitations cause problems. The quantity of RF chains, phase shifters, and power amplifiers has a major impact on the effectiveness and power consumption of beamforming in hybrid-electrical systems. It is also important to think about how effective the phase shifters are. Compared to previous methods, hybrid beamforming needs more radio frequency (RF) components and high-speed data converters to manage multiple streams efficiently. Determining channels and creating beams becomes significantly more challenging when there are multiple antennae . The need to balance system performance and processing complexity means that there are not many practical options. We must continue to study these issues in order to develop beamforming methods that are effective and widely applicable. To address these issues, new methods for signal processing and hardware design are required. By applying advances in ML and adaptive algorithms, we may discover new ways to optimize performance while reducing complexity in hybrid beamforming systems.

2.3 COMPARISON OF ADVANTAGES AND LIMITATIONS

Traditional beamforming techniques need static system parameters that cannot adjust to changes in the environment. Although the system performs better when the settings are adaptively adjusted, this also raises the possibility of overfitting, which complicates things. makes it is more difficult to use what have learned in novel circumstances [2]. Even if the system parameters are not measured with great precision, strong beamforming solutions may still function well. But they mostly depend on knowing how the desired parameters are spread out, and they often get confused when the model doesn't fit well. Also, strong methods often give safe answers and may not work as well as weak methods when there is no steering vector mismatch. Making durable beamformers that don't care about array steering vector mismatches with unknown deterministic forms is hard.

Digital and analog hybrid designs take the best parts of both types of structures and combine them to make full digital beamforming with fewer radio frequency (RF) links. This cuts down on hardware costs by a lot [6]. But right now, hybrid beamforming methods need CSI at the transmitter, which adds more work that doesn't get easier as the number of antenna parts grows. Using phase-shifters with the same preset attenuation for all channels is also the easiest way to do things right now. This makes the spatial direction and the spectrum efficiency worse.

Standard beamforming techniques offer fixed weight vectors that do not adapt dynamically to environmental changes. But recent AI and ML algorithms can change with the radio environment. This helps to find a good middle ground between the performance is needed and the difficulty of putting it into action [4]. These methods make beamforming more flexible by using the fast convergence rates and efficient computing of ML and DL algorithms.

2.4 BEAMFORMING IN 5G AND EMERGING 6G SYSTEMS

The article focuses on advanced beamforming technology poised to increase 6G performance via smarter and more efficient usage of the frequency band. Varieties of beamforming solutions have been considered for both 5G and 6G systems, such as analog, digital, and hybrid variants. Further gains can be achieved through adaptive and robust beamforming with AI/ML algorithms. With massive MIMO technology, a large number of communications–frequency bands can share a common time slot using the shortest available wavelengths in the terahertz frequency bands in 6G communications. To improve coverage, capacity, and spectral efficiency, new technology in 6G communications introduces reconfigurable intelligent surfaces, sub-arrays, and ultra-massive MIMO antennae .

2.4.1 Massive Mimo and Its Impact on Spectral Efficiency

A massive-MIMO scheme incorporates large antennae amount in base stations to connect with multiple devices concurrently. Such systems are very important in networks operating with millimeter and terahertz wave communications, which offer record-breaking spectral efficiency and greatly reduced interference. Such systems can provide a targeted beamforming technique to eliminate interference effects for individual devices, allowing flexible usage of the whole frequency band. Future 6G communications will allow a peak speed of 1 terabit/second, which will be possible because THz communications will support over 1 exabit/second per cubic meter. Reconfigurable intelligent surfaces, ultra-massive MIMO systems, and multi-sensory holographic radio systems are major enablers of THz communications [9].

2.4.2 Millimeter-Wave and Terahertz Beamforming

In 6G systems, it will be possible to communicate in the terahertz and millimeter-wave bands. This will give users access to a lot of interesting resources. Nonetheless, the path loss in these bands is substantial enough to necessitate beamforming. This makes up for the loss of transmission by focusing the signal strength into a tight beam at the antenna. New ways of beamforming are needed to make 6G terrestrial wireless networks more efficient in terms of spectrum use. It can be used very large antenna arrays in higher frequency bands, which helps with spectral efficiency, connection reliability, and dealing with interference. With fully digital beamforming, it can be controlled the phase and amplitude of the signal at each antenna very precisely. This lets to have many separate beams at once. But each antenna needs its own radio frequency (RF) chain, which makes the hardware costs and power use very high. It costs less to use a single RF chain for fully analog beamforming, but it can only make one beam, so it can't handle more than one stream or serve more than one user. Hybrid beamforming, which uses a few RF chains and phase shifters, is a middle ground that lets to do multi-beamforming without spending too much on hardware and power [10].

2.4.3 6G Innovation Keys

A 6G-networks are the sixth version of cellular wireless knowhow. It wants peak data speeds of many terabits per second, latency of less than a millisecond, and the ability to combine AI with intelligence that is everywhere. People think that the main communication range is between 250 GHz and 3 THz. Reconfigurable intelligent surfaces, ultra-massive MIMO, AI-assisted network design, the combination of communication, sensing, and computation, and the use of blockchain are some of the most important new features of 6G. Some important performance indicators are the data rate, communication latency, user experienced information rate, energy efficiency, spectrum efficiency, connection density, dependability, localization accuracy, and intelligence level. 6G plans to use the Terahertz (THz) band for ultra-massive multi-antenna communication systems. This is because future networks will need to use their spectrum more efficiently. They will eventually be able to accommodate an increasing number of devices and applications thanks to their efficiency, which will improve user experience and connectivity. Finding creative solutions for spectrum management will become more and more important as technology develops. This strategy expands on previous 5G efforts, such as the use of the 6 GHz to 100 GHz frequency spectrum and extensive MIMO deployments with up to 256 antennae [11]. We anticipate that these developments will open the door for even more cutting-edge technologies, allowing for faster data speeds and better connectivity. Improved applications, such as smart cities, driverless cars, and cutting-edge telemedicine technologies, will thereby help industries.

2.5 SPECTRAL EFFICIENCY IN WIRELESS NETWORKS

Networks for wireless communication are constantly evolving to meet the increasing demand for data. Massive MIMO arrays and additional frequency bands have allowed networks to grow in size and improve their data transmission capabilities. In order to serve more users simultaneously and offer faster data speeds and better service, the next 6G standard will require a large number of antennae and capacity. In order to maximize performance and resource allocation as technology develops, network management will need to incorporate AI. In addition to improving user experience, this evolution will make it possible for seamless connectivity across a range of platforms and devices. Therefore, a high level of spectral efficiency is essential for future mobile networks. By examining the spectral efficiency, it may determine how well frequency resources are being used to transmit data. Faster speeds and better service quality result from higher spectral efficiency, which allows more data to be sent over the same bandwidth. In order to fulfill user expectations and enable developing technologies, network operators will need to optimize spectral efficiency as the demand for mobile data continues to rise. In addition to improving user experiences, this optimization will save providers money on operating expenses. The sector can maintain its agility and responsiveness to the changing landscape of digital communication by investing in cutting-edge technologies and creative solutions. The maximum bit rate per unit of bandwidth that an internet connection can manage is one approach to gauge these qualities. Numerous factors, including beam alignment, interference levels, availability of CSI, and the precision of CSI estimations, influence the spectral efficiency of 6G frequency bands. Therefore, improving spectral efficiency may greatly benefit from reducing the angle error between the antenna's main lobe and the LoS route as well as identifying methods to reduce interference. Optimizing these parameters can also be greatly aided by developments in ML algorithms and adaptive beamforming technologies. Networks can greatly improve their performance and dependability by continuously assessing their surroundings and modifying the beam patterns in real time. Beamforming techniques that were employed in 5G may be modified to improve spectral efficiency in 6G scenarios. For instance, the FS-HBF technique eliminates inter-symbol interference in wideband THz MIMO channels by combining hybrid beamforming and fractional delay techniques [7]. In the absence of precise CSI, an adaptive MIMO beamforming system may use iterative algorithms to determine optimal topologies by reducing the mean square error between broadcast and received signals [6]. Other methods such as precoding systems, multi-user arrangement, cooperative-beam navigation, and power-allocation may also donate to the spectrum's increased efficiency when combined with beam alignment and tracking protocols.

2.6 CHALLENGES

It is hard for entirely digital beam routing to work well and be useful because of hardware limits. One thing that is hard to do when there are hundreds of antennae is make sure that the RF chains number is the same as the number of transmit antennae [1]. Phase shifters or switches are used in an analog RF beamformer and a low-dimensional digital beamformer to make hybrid beamforming work [4]. But there are still problems with hybrid designs, like having too few RF chains, phase shifters that aren't very accurate, and not being able to control the amplitude of each antenna.

2.6.1 Hardware Limitations

To maximize spectrum use, progressive beams routing methods are now needed in the terahertz and millimeter-wave domains. For umMIMO systema with extremely severe hardware constraints, hybrid beamforming has been studied. To improve the accuracy of angle prediction, beam tracking and channel estimation have been included [1]. When it uses big arrays, hardware problems are very important. Hybrid architectures use fewer radio frequency (RF) chains than setups that are only digital. Compared to traditional phase shifter designs, switch-based systems may also cut down on hardware costs and power use [4]. But it costs a lot of money, power, and work to put phase shifters on all of the antenna elements. For analog-only systems, there must be a one-to-one relationship between RF chains and antenna elements. This makes them less adaptable. The shape of the array, the bandwidth, the number of active RF chains and antennae, subarray partitioning, modulation gains, the distance between antenna components and subarrays, and random calibration errors all have an effect on beamforming's properties and strength. It is still hard to find the best array designs, and performance is often measured by the ratio of signal/interference with plus-noise or spectral efficiency measures. There is no single answer that works for everyone. If the angle and CSI are wrong, the beamforming gain might go down. This means that if it uses PI controllers correctly, they might be able to fix these problems. However, complicated feedback systems and other factors that affect them lower loop gains, which makes them less effective. The development of adaptive and resilient beamforming methodologies mitigates these shortcomings; however, the digital architecture of fully adaptive systems demands considerable hardware complexity, especially in large and ultra-large arrays.

2.6.2 Channel Estimation Errors

As early as this time, the use of innovative concepts through the development of adaptive and high-performance beamforming techniques has resolved the shortcomings associated with the older direction of arrival techniques. AI and ML are becoming increasingly prevalent in various systems, owing to their ability to utilize numerous parameters to enhance performance [16]. Although these technologies are rapidly evolving, there are still many significant challenges associated with implementing AI/ML in conjunction with a large Antenna Array due to the costs associated with training and the difficulty associated with using these systems. In the case where reducing complexity or overhead is the principal requirement, Conventional Beamforming Systems can still be employed in this case. Examples of these systems include but are not limited to mMIMO Systems; each of these employs a significant number of Antenna Elements to create multiple beams in High Frequency Communication Channels. Beamforming techniques are necessary because of the high levels of signal degradation at both the mmWave and Sub Terahertz Bandwidth frequencies. Ultra-Massive Antenna Arrays provide the Spatial Degrees of Freedom required to address these issues. By the time of 6G and beyond, the implementation of 3D Massive MIMO has transformed into umMIMO and Intelligent Surfaces, thereby enabling improved Beamforming in Large Dimensional Spaces. Hybrid analog and digital Beam forming Designs allow significant amounts of dimensional Beamforming, while using fewer & lower power RF Front Ends. These two types of technology, hybrid analog and digital Beamforming, can both work together to create an improved coverage and spectrum efficiency within 6G wireless communication systems. Beamforming is one of the most important technologies for achieving greater spectral efficiencies in 6G wireless communication networks due to their use of ultra-massive antenna arrays. The amount of spectrum used effectively in a wireless network can be measured in bit/s/Hz. The amount of spectral efficiency that 6G Wireless Communication Networks can achieve depends heavily on the number of array beams routing vector targets (beam alignment), the interference level experienced between different users, the accuracy of the antenna arrays, and the quality of the CSI provided to the transmitter. If the transmitter has completed and accurate CSI, it is possible to simultaneously construct the two types of Beamformers, transmit and receive Beamformers, by employing Pre-coding techniques and High-dimensionally Multi-user Scheduling. But even when there is limited availability of CSI, collaborating with other base stations to conduct Beamforming could still improve spectral efficiencies for users [18].

2.6.3 Trade-offs between Beamforming Complexity

In order for the RF signal to accurately travel from an antenna(s) to its intended destination, it is necessary to have some method of directing or focusing the RF signal. Anti-adiabatic beamforming solves this issue by allowing for the adaptive change in direction of an RF signal or "beam." There are three general types of beamformers used by communication systems: analog, digital, and hybrid. Both Analog and Digital Beamformers have been used with success at lower frequency ranges; however, the Hybrid Beamformer is anticipated to be effective for future applications such as millimeter wave (MIMO) technology [9]. Hybrid Beamforming requires fewer RF chains than other types of Beamformers which creates a good balance between hardware cost/resource requirements and performance. The Generalization of the H-Beam forming method has opened up many possibilities for future development with more elaborate methods being developed. Examples include Adaptive Beamforming and Robust Beamforming [4]. The concept of Adaptive Beamforming utilizes a set of "weights" to maximize the strength of the RF beam in the desired signal direction while reducing the beam toward interference and noise. Robust Beamformers focus on reducing interference when there are steering vector mismatches between the true RF beam direction and the assumed RF beam direction. Many companies and research institutions are now utilizing AI and ML techniques and tools to design and implement Adaptive Beamforming and Robust Beamforming techniques [2].

2.7 RELATED WORK AND COMPARATIVE ANALYSIS

Advanced research activities have highlights on investigation of new beamforming techniques that can enhance spectral efficiency (SE). Hybrid beamforming based on multi-phase-rotation of the analog signal was introduced [7]. The method can suppress multi-user scenarios in inter-user interference. Beams navigation algorithm for directional multiple-input multiple-output (MIMO) antenna arrays in 5G systems was presented. Two methods are proposed: one balances between error vector magnitude and SE; the other maximizes SE [1]. Further enhancement of SE was achieved based on a DFT-based analog system that combines different hybrid beamforming structures, and a robust beamforming technique that considers channel uncertainties. A further advance involves factorizing the resultant digital beamforming weights to feed multiple analog arrays simultaneously; this extends SE gains and reduces RF-chain overhead. These concepts were then integrated to form a novel analog architecture with digital beamforming decomposition requiring only a small number of phase-shifters.

2.8 SUMMARY OF LITERATURE REVIEW

Conversely, hybrid beamforming achieves a balance between spectral and energy efficiency. Although it achieves near-optimal performance compared to digital beamforming, it requires only a few RF chains, reducing power consumption and hardware complexity [20]. Adaptive beamforming allows antenna arrays to change their pattern based on the surrounding environment in order to minimize interference and maximize the desired signal from intended directions while suppressing signals from others [12]. Robust beamforming is suitable for situations where the CSI is uncertain or imperfect. These algorithms use different optimization models to design beamformers that are not sensitive to CSI errors and can maintain good performance [19]. AI/ML-based beamforming utilizes ML techniques such as deep learning and reinforcement learning to learn and optimize beamforming strategies from data, adapting to complex wireless environments. A comparative analysis of 25 recent works on Backscatter-Assisted NOMA for Ultra-Massive Machine-Type Communications (UM-MTC) in 6G networks highlights significant trends and research deficiencies. Wi-Fi, LTE, and TV spectrum are all examples of new technologies that work at frequencies lower than 6 GHz. They disperse and blend quite effectively with other noises, which explains this. However, recent research indicates a distinct trend toward frequencies operating at millimeter-wave (mmWave) and terahertz (THz) levels. While higher frequencies have larger bandwidths and improved spectral efficiency, the passive tags suffer from a significant loss in signal strength and are limited by strict energy constraints. Researchers are therefore looking at creative ways to improve passive tags' performance in these difficult settings. They seek to get beyond current restrictions and improve communication over these higher frequency ranges by utilizing cutting-edge materials and signal processing techniques. There is a lack of thorough hardware measurements, such as antenna gain and tag dimensions, despite theoretical research suggesting that NOMA-assisted backscatter might greatly expand the spectrum. This case illustrates how analytical modeling and real-world implementation are not necessarily compatible. Experimental research that supports theoretical predictions and improves hardware designs is essential to addressing this discrepancy. By focusing on real-world implementations, researchers can better understand the challenges and potential of NOMA-assisted backscatter in practical scenarios. Backscatter tags that are commonly used have gains between -3 dBi and +4 dBi and footprints that are only a few millimeters wide. As a result, many people are now looking for designs that use graphene or metasurfaces to make small antennae with a lot of gain. The majority of the systems examined are appropriate for low-rate IoT applications, given that ambient bandwidths range from 5 to 20 MHz, but are not suitable for UM-MTC. People don't often consider energy harvesting, security, and interference management all at once, even though they are all essential for big 6G networks. There are only a few papers that talk about how to use Reconfigurable Intelligent Surfaces (RIS) or STAR-RIS to improve coverage and reflection. The whole study shows that future 6G systems will need to have AI-based adaptive control, hybrid frequency operation, and energy-efficient hardware to make backscatter-NOMA communication reliable, high-capacity, and safe for connecting many devices. This creative method will probably completely change how we think about resource allocation and network design. We may anticipate major developments as academics continue to investigate these technologies, which will improve connectivity and meet the expanding needs of a world that is becoming more and more digital. These advancements will improve network performance and open up new applications in the IoT, smart cities, and driverless cars. A future of seamless connectivity is predicted by utilizing AI and cutting-edge communication technology, which will promote smarter infrastructure and effective resource management. In the end, this evolution might result in sustainable urban development and increased societal involvement by fostering cross-sector collaboration, fostering innovation, and tackling urgent global issues.

Table 2.1: Critical Observations and the Need for Proposed Research.

No.	**Reference (title)**	**Frequency (band used / targeted)**	**Bandwidth**	**Gain (reported / typical)**	**Size (reported / typical)**	**Applications**
1	Backscatter-NOMA: An Integrated System of Cellular and IoT Networks (ICC 2019). (ResearchGate)	Cellular / sub-6 GHz (integrates cellular carriers)	system-level (carrier BW)	not specified — typical 0–6 dBi for tags. (ACM Digital Library)	tag: tiny (cm scale) — not specified. (ACM Digital Library)	Cellular + passive IoT, uplink capacity with NOMA. (ResearchGate)
2	NOMA-Enhanced Backscatter Communication for Green IoT (2019). (White Rose Research Online)	Wi-Fi / sub-GHz / cellular (paper discusses general AmBC bands)	depends on ambient source (e.g., 20 MHz Wi-Fi)	not specified — typical. (ACM Digital Library)	small RF tag (cm scale). (ACM Digital Library)	battery-free IoT uplink, energy-efficient mMTC. (White Rose Research Online)
3	A survey on ambient backscatter communications (2022) — comprehensive survey. (ACM Digital Library)	Ambient bands: TV (VHF/UHF), cellular sub-6 GHz, Wi-Fi (2.4/5 GHz), BLE. (ACM Digital Library)	ambient source dependent (kHz→tens of MHz)	typical tag gains: −2 to +4 dBi. (ACM Digital Library)	tag antenna footprint: mm → cm scale. (ACM Digital Library)	Ambient backscatter for indoor sensing, asset tracking, mMTC. (ACM Digital Library)
4	Performance Analysis of Ambient Backscatter-NOMA (Applied Sciences 2023). (MDPI)	AmBC over common ambient carriers (2.4 GHz / cellular referenced)	uses ambient carrier BW in analysis (e.g., 20 MHz example)	not specified in formulaic analysis. (MDPI)	not specified — assumed small tags. (ACM Digital Library)	AmBC-NOMA outage / ipSIC analyses for mMTC scenarios. (MDPI)

Table 2.1: Critical Observations and the Need for Proposed Research (Table Continued).

5	Backscatter Assisted NOMA-PLNC Based Wireless Networks (Sensors 2021). (MDPI)	sub-6 GHz (paper system model)	system-level (not hardware BW)	not specified — assumed small tag antennae. (MDPI)	tag: compact (paper-level assumptions). (MDPI)	Low-power 5G scenarios, IoT uplink enhancement. (MDPI)
6	Joint optimization for secure ambient backscatter NOMA (ScienceDirect / 2023). (ScienceDirect)	AmBC with cellular/Wi-Fi ambient carriers (sub-6 GHz)	ambient BW (depends on source)	not given (focus on optimization). (ScienceDirect)	tag small; not detailed. (ACM Digital Library)	Secure AmBC-NOMA in presence of eavesdroppers. (ScienceDirect)
7	Cooperative backscatter NOMA with imperfect SIC (2022). (ScienceDirect)	sub-6 GHz modeling (system-level)	not specified	not specified — system model. (ScienceDirect)	not specified	Cooperative NOMA + backscatter; resource management for 6G. (ScienceDirect)
8	Ambient Backscatter Communications: A Contemporary Survey (2018). (ResearchGate)	Wi-Fi (2.4/5 GHz), TV bands, BLE, cellular	ambient-dependent	typical tag antenna gains −3 → +3 dBi. (ResearchGate)	antenna tags — few cm. (ResearchGate)	foundational AmBC use-cases: sensing, passive IoT. (ResearchGate)
9	Resource Allocation in NOMA-Assisted Ambient Backscatter (2021 thesis/paper). (espace2.etsmtl.ca)	AmBC over ambient carriers (system analysis)	ambient BW referenced (varies)	not specified	tag/device size not specified	resource allocation / sum-rate maximization for AmBC-NOMA. (espace2.etsmtl.ca)
10	A distributed perspective on Backscatter systems (arXiv 2025) — systems survey. (arXiv)	multi-band overview (TV / cellular / Wi-Fi / LoRa)	varies widely — survey	gives typical ranges for tags based on literature. (arXiv)	discusses deployments — tag footprints cm→tens cm. (arXiv)	mMTC, distributed backscatter networks, system-level design. (arXiv)

Table 2.1: Critical Observations and the Need for Proposed Research (Table Continued).

11	Ambient backscatter communications over NOMA downlink (Semanticscholar). (Semantic Scholar)	Typical AmBC bands (2.4 GHz / cellular)	ambient BW dependent	not specified	not specified	NOMA downlink riding ambient backscatter (commensal AmBC). (Semantic Scholar)
12	Joint Optimization for Secure Ambient Backscatter (arXiv 2021). (arXiv)	sub-6 GHz ambient carriers in security model	depends on ambient source	not specified	not specified	PHY security frameworks for AmBC-NOMA. (arXiv)
13	Performance of AmBC-Assisted NOMA signalling in an mMTC network (2025 preprint / conf.). (ResearchGate)	modeled for mMTC — sub-6 GHz assumptions	uses short-packet regimes (BW depends on carrier)	not hardware-specific	tag small — assumed	AmBC + NOMA for mMTC short-packet performance. (ResearchGate)
14	mmWave Backscatter survey (2024) — mmWave BackCom overview. (ScienceDirect)	mmWave bands (e.g., 28–60 GHz)	wider bandwidths (hundreds of MHz to GHz)	tag gains vary (directive arrays possible)	tag/array size: mmWave tags can be small but antenna arrays may be larger	mmWave backscatter for high-rate sensing, and potential UM-MTC hotspots. (ScienceDirect)
15	STARS-aided NOMA ambient backscatter (2024). (ScienceDirect)	system uses RIS/STARS + AmBC (sub-6 GHz / configurable)	depends on ambient	not specified (system level)	not specified	RIS/STARS enhanced AmBC-NOMA — coverage/BLER improvements. (ScienceDirect)

Table 2.1: Critical Observations and the Need for Proposed Research (Table Continued).

16	Backscatter-assisted non-orthogonal multiple access network (IET 2023). (IET Research Journals)	sub-6 GHz modeled (system level)	not hardware BW specific	not specified	small tags	uplink assistance using backscatter with NOMA for rate maximization. (IET Research Journals)
17	NOMA-Based Backscatter Communications (IEEE/TechRxiv review). (TechRxiv)	overview across ambient carriers (sub-6 GHz, Wi-Fi, TV)	ambient BW dependent	typical tag gains cited from literature. (TechRxiv)	tag size typical cm scale	review of NOMA+Backscatter use cases and open problems. (TechRxiv)
18	Simultaneous Harvest-and-Transmit Ambient Backscatter (2019). (DNB)	AmBC on Wi-Fi / TV / ambient carriers (paper examples)	ambient BW dependent	not specified	tag energy-harvesting form factors (small)	EH + AmBC design for pervasive IoT connectivity. (DNB)
19	Review: Development in ambient backscatter communications (IET 2023). (IET Research Journals)	Wi-Fi, Bluetooth, TV — indoor/outdoor ambient carriers	depends on ambient source	typical tag antenna gains and sizes covered. (IET Research Journals)	tag sizes cm scale for indoor devices. (IET Research Journals)	indoor sensing, battery-free sensors, mMTC. (IET Research Journals)
20	BLER performance in RIS-assisted ambient backscatter (PLOS One 2025). (PLOS)	AmBC + RIS — paper uses specific carrier examples (sub-6 GHz/2.4 GHz)	short-packet BW choices in study	not hardware-focused	tags small; RIS large planar. (PLOS)	URLLC / short-packet AmBC-NOMA with RIS assistance. (PLOS)

Table 2.1: Critical Observations and the Need for Proposed Research (Table Continued).

21	A Survey of mmWave Backscatter: Applications, Platforms (2025). (ACM Digital Library)	mmWave bands (tens of GHz)	hundreds of MHz → GHz	tag/array gains vary; can be directive	mmWave backscatter tag/element scales vary; arrays larger	high-rate sensing, short-range UM-MTC hotspots. (ACM Digital Library)
22	Review on LoRa Backscatter (2025). (ScienceDirect)	Sub-GHz LoRa bands (e.g., 868/915 MHz)	LoRa channel BW (125/250/500 kHz typical)	tag gains typical for sub-GHz antennae (0–3 dBi)	tag antennae: few cm to tens of cm depending on tuning. (ScienceDirect)	LPWAN passive IoT, long-range low-data mMTC. (ScienceDirect)
23	Green designs for Energy Harvesting in BackCom (MDPI Energies 2025). (MDPI)	multi-band (survey)	depends on ambient source	reports typical EH tag antenna efficiencies / sizes	discusses tag form factors and EH hardware	energy-harvesting backscatter for sustainable IoT / UM-MTC. (MDPI)
24	Backscatter-NOMA: A Symbiotic System (Semantic scholar summary). (Semantic Scholar)	cellular / Wi-Fi bands in analysis	system level — ambient BW examples	not specified	tag small — assumed	symbiotic cellular + passive IoT using NOMA. (Semantic Scholar)
25	Resource/Optimization papers (e.g., IEEE/MDPI/ArXiv works on AmBC-NOMA 2020–2024) — representative cluster. (TechRxiv)	sub-6 GHz / Wi-Fi / TV depending on study	ambient BW dependent (20 MHz Wi-Fi, etc.)	typically, not hardware-specific	typical tag: cm scale; may assume isotropic or small patch antennae. (ACM Digital Library)	optimization, resource allocation, security, SIC impairment modeling for AmBC-NOMA in mMTC/UM-MTC. (TechRxiv)

3. RIS SYSTEMATIC DESIGN

A new technology called Intelligent Reconfigurable Surface (IRS) antenna array systems has the potential to revolutionize communication. Conventional wireless communication systems begin to encounter issues when the demand for higher data speeds, improved coverage, and lower energy consumption grows. IRS antenna arrays are a novel application of reconfigurable surface technology to enhance wireless communication systems. More sophisticated KPIs [1] and a greater variety of new use cases will be made possible by the upcoming 6G network standard. Sixth-generation (6G) networks require a new way to transmit and receive data, as well as to sense, communicate, process, and, most critically, operate together in a programmable environment [2]. Over the last several decades, a number of technological advancements have moved mobile communications forward [3]. Designers have been making high-efficiency transceivers for years to make up for signal loss at the ends of a radio channel. Now, as they get ready for 5G technology, they are starting to realize that they have hit the realistic limits of transceiver efficiency [4]. The fifth generation of communication systems must fulfill a lot of criteria, such very high data rates, great mobility, and low latency, which are not accessible in older networks [5]. Tele education, virtual reality workplaces, social networking, telemedicine, e-governance, e-commerce, and many more new applications that use a lot of data will need these standards [6]. For such a broad variety of uses, a high-gain antenna array is quite useful [7]. To meet the huge demand for high-volume data transmission over the communication channel, multiple-input multiple-output (5G) antennae are used. This is because they allow it to use data faster, they require less power than the data rate, and they are not impacted by multipath fading [8]. Resource distribution may pose a significant optimization problem in the context of 5G networks, requiring effective solutions [9]. To guarantee peak performance, these solutions must strike a balance between user demand and available resources. Moreover, the requirement for adaptive algorithms to preserve service quality grows as user density rises. Distributed optimization is one of the most used approaches to optimization issues. Several network nodes collaborate to find the optimal response in this approach [10]. Among these algorithms is the Alternating Direction Method of Multipliers (ADMM) [11]. [12] claims that ADMM is a distributed optimization technique that can assist in resolving issues in communication networks that call for resource participation. Dividing the optimization problem into smaller components is a good concept [13]. In a 5G network, ADMM can be utilized to supply various users with radio resources, such as bandwidth and power [14], [15]. The ADMM algorithm performs the following functions: By dividing the issue into smaller components, each can be handled independently by a different node in the network [16]. After resolving its own little issue, each node reports its findings to the other nodes in the network [17]. Because nodes can work independently and still contribute to the overall goal, this cooperative approach increases efficiency and speeds up processing time. As a result, the network can adjust more quickly to changing user demands, guaranteeing efficient use of resources. As a result, neighboring nodes can exchange information and modify their responses as necessary [18]. Until it converges, the process will continue [19]. With frequent convergence and low communication overhead, ADMM has shown itself to be a successful strategy for resolving resource allocation issues in 5G networks [20]. Additional distributed optimization techniques that are effective for resource sharing in 5G networks are the distributed sub-gradient method and the primal-dual gradient approach [21]. Distributed optimization is demonstrated by both of these. By increasing scalability and efficiency, these techniques enable networks to adjust to changing demands and circumstances. More developments in distributed optimization methods will be essential for maximizing efficiency and resource use as the telecom industry changes.

3.1 METHODOLOGY AND DETAILS

The numerical approach makes use of a fictitious simulation environment to simulate and enhance the IRS antenna array's performance. Without being constrained by real-world circumstances, this environment enables researchers to test different shapes and parameters. They can choose the best designs that improve coverage and signal quality by examining the data. Researchers can use CST MWS, a popular technique for modeling electromagnetic fields, to investigate and construct complicated structures with high precision. This is the course of action that the Internal Revenue Service ought to take. This method reduces the dangers connected with physical testing while saving time and money. In the end, using such sophisticated modeling techniques might result in creative fixes and better results across a range of applications. Intelligent IRS aims to employ CST MWS to build a virtual simulation environment where users may perform modeling and optimization activities and learn about the IRS antenna array. This novel method not only improves comprehension of the IRS antenna array but also enables controlled testing and real-time changes. Both professionals and students can benefit greatly from this dynamic atmosphere, which promotes experimentation and a deeper understanding of difficult ideas. Users can hone their abilities and create strategies as they interact with the simulation that would not be possible in real-world testing situations. Users can experiment with different shapes by utilizing CST MWS's capabilities, which will ultimately result in more effective designs and enhanced performance. Through the use of accurate electromagnetic simulations, design theory seeks to provide precise wavefront regulation, beamforming modification, energy conservation, and operation with current communication networks. Before implementing intelligence IRS systems with CST MWS, they are simple to develop and test. A more thorough examination of the recommended approach is provided in Figure 1. The construction of intelligent IRS antenna array systems that do numerical simulations is demonstrated in this flowchart using CST MWS. Through the optimization of design parameters made possible by these simulations, the systems' ability to adjust to changing environmental circumstances and user needs is guaranteed. By incorporating real-time data, these intelligent IRS systems operate even better, leading to increased dependability and efficiency in communication. Setting the material and shape parameters is the first step. Determining how electromagnetic waves pass through the material is the next stage. Channel estimation, beamforming, wavefront modification, and feedback can all be simulated with reconfigurable element models and intelligent control algorithms. The approach continues to improve the IRS. It tests the design's compatibility with energy efficiency, security, privacy, and communication networks before it is finalized. Making an IRS array that functions well with mmWave bands is demonstrated in the flowchart. It has two paths that run next to each other: an IRS route that makes the array work better for mmWave operation and matches it to its intended uses, and an array path that makes the array work better for mmWave operation. This can check to see if the optimization meets the requirements at each decision point along the way. The procedure works well, the proposed IRS array is added, and a final choice checks to see if the new design improves things. The picture has a simple blue and white color scheme, with clear rectangular process boxes and decision nodes that look like diamonds. Figure 3.1's flowchart shows how to make an IRS array that works with mmWave technology.

a. The first step is to make two parallel paths: one for the first design of the IRS and the other for the first design of the array.

b. First, make the IRS work better for mmWave bands, and then test it in an array setup.

c. Make sure the array works with the apps it desires it to work with and that it works well with mmWave.

d. There is a point on each route where its container check to see if the optimization meets your needs.

e. After both pathways are finished, the next step is to add the proposed IRS array.

f. The last evaluation checks to see how much better the new design is than the old one. If the answer is yes, the process is done; if not, more work needs to be done to make it better.

g. The figure is blue and white and has rectangular process boxes and diamond-shaped decision nodes that make it look more professional and easier to read.

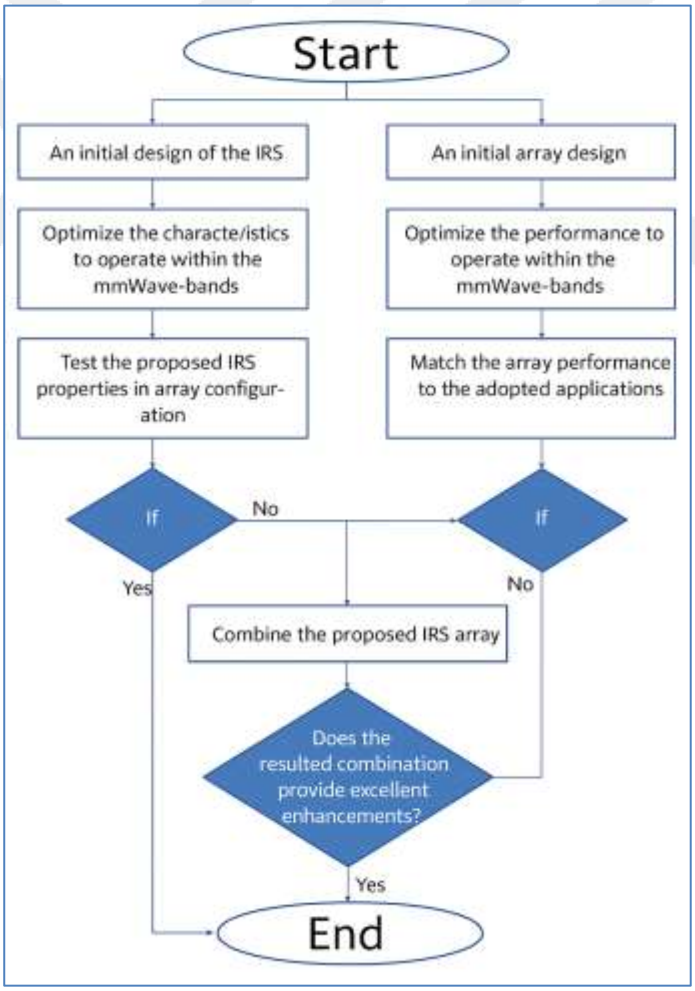

Figure 3.1: Methodology and Details.

3.2 IRS DESIGN GEOMETRICAL DETAILS

The proposed IRS design is as Sikrpency quadrature flower-based bowtie unit cells. The proposed unit cell occupies a size of 5mm2 to provide a frequency resonance at 26GHz with a bandwidth of 2GHz bandwidth. The individual unit cell provides a gain of 4dBi. The proposed unit cell is arranged inside a 2D array of 100×100 shape. Also, the resulted array performance can be controlled using varactor diodes that realize a phase shit progressive to maintain the ability of beam forming and steering to the desired location. In such geometry the proposed unit cell is designed as Sikrpency quadrature flower bowtie [22], see Fig. 3.2, to ensure bandwidth enhancement and gain improvements. The proposed structure based on a Sierpinski fractal antenna design is implemented in MATLAB. In this design, we have to keep in mind that this code is a basic example and might require further refinement for specific applications.

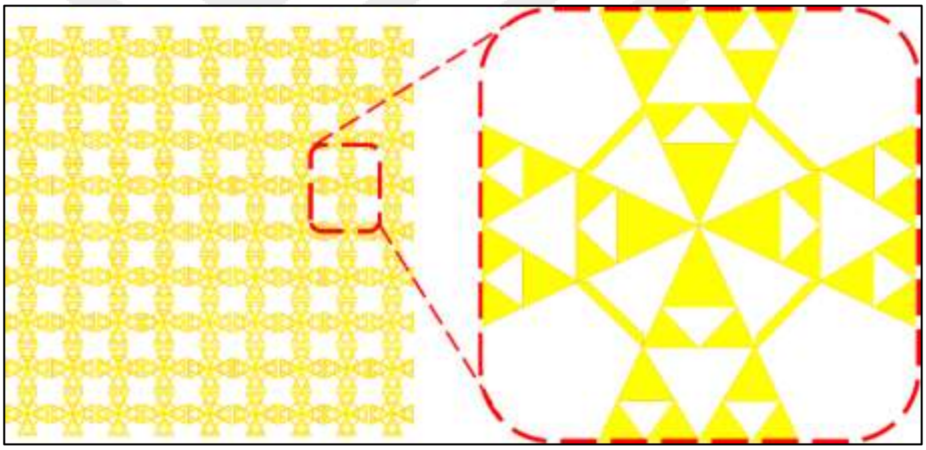

Figure 3.2: IRS Layer Based on Array Shape from CST MWS.

3.2.1 Single Element

The single element is intended to function at resonance frequencies of 26GHz. Figs. 3.3(a) and 3.3(b) depict the geometry of the suggested single antenna patch element. The Rogers family RO 3003 lossy patch design with a dielectric constant of three is installed on a substrate that is 1 mm thick. A ground plane measuring 4x4 mm2 and made of copper material with a width of 0.035 mm provides full support for the rear board of the proposed antenna. The antenna patch is made of copper and is 5 mm by 5 mm. It is 0.035 mm thick. Table I lists the geometrical parameters of the suggested antenna. A coaxial probe feed is used to leave the antenna element. At 0.45 mm from the patch edge, the feed placement is set to the antenna's x-axis. The frequency-band of notice has a fixed co-axial prob input impedance of 50 ohms. The following equations are used to analytically determine the antenna element sizes [23].

$$\epsilon_{reff} = \frac{\epsilon_r+1}{2} + \frac{\epsilon_r-1}{2}[1 + \frac{12h}{w}]^{-1/2} \tag{3.1}$$

$$\Delta L = h\ x\ 0.421 \frac{(\epsilon_{reff}+0.3)(\frac{w}{h}+0.264)}{(\epsilon_{reff}-0.258)(\frac{w}{h}+0.8)} \tag{3.2}$$

Where ϵ_r is the dielectric continuous, w is the thickness of the radiating part, and h is the height of the substrate. The actual length of microstrip patch is stated as [24].

$$L = L_{eff} - 2\Delta L \tag{3.3}$$

Finally, the effective length and width of the patch are calculated as [25]

$$L_{eff} = \frac{v0}{2f_r\sqrt{\epsilon_{reff}}} \tag{3.4}$$

$$W = \frac{vo}{2f_r}\sqrt{\frac{2}{\epsilon_r+1}} \tag{3.5}$$

These limits are used as initials to behavior a parametric training based on the numerical examination to be enhanced to achieve the wanted presentation. All these dimensions values have a remarkable effect on the antenna routine.

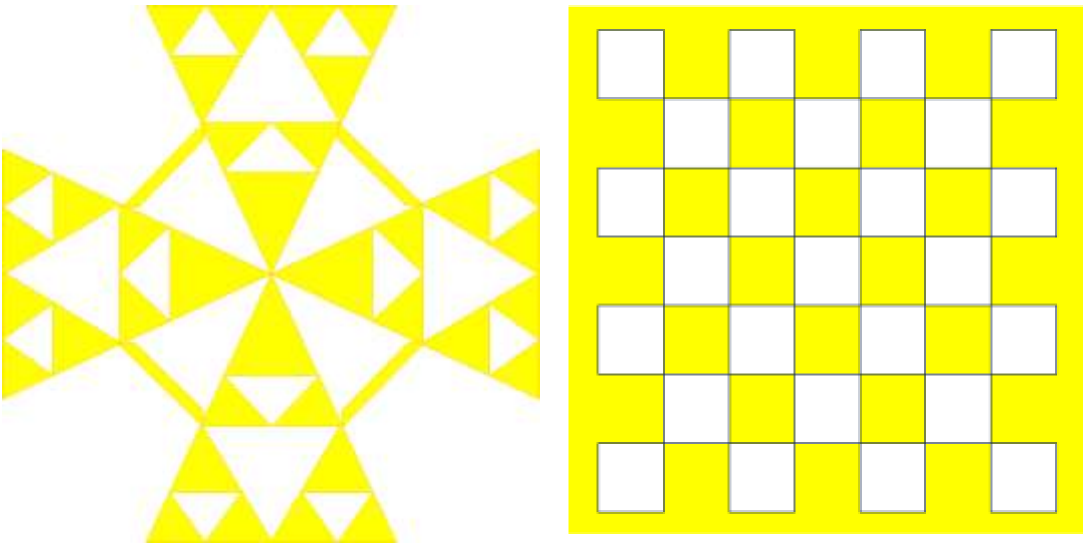

(a) (b)

Figure 3.3: Unit Cell Design from CST MWS: (a) Front View and (b) Back View.

3.2.2 Array Shape

Array antenna skill is a compelling application, as contemporary communication systems require steerable antenna systems, high-gain arrays, and enhanced radiation patterns. The proposed antenna element, shown in Fig. 3.4, reaches a peak gain of 6.97dBi at 26 GHz in our design. Due to propagation restrictions, such gain is insufficient for mm-wave technology. Consequently, a one-dimensional array configuration is proposed to circumvent the antenna gain limitation [26]. The eight components constituting the proposed antenna element are randomly distributed along the x-axis. The selected spacing between the elements is ($\lambda/2$). Figure 3.4 illustrates the geometry of the array [27]. The observations of the antenna elements were consolidated to ascertain the overall pattern and gain [28].

Table 3.1: Geometrical Parameters of the Antenna.

Parameter	**Value (mm)**
thickness Substrate	1
length Substrate	6
width Substrate	6
length Patch	5
Patch width	5
Patch thickness	0.035
Ground thickness	0.035

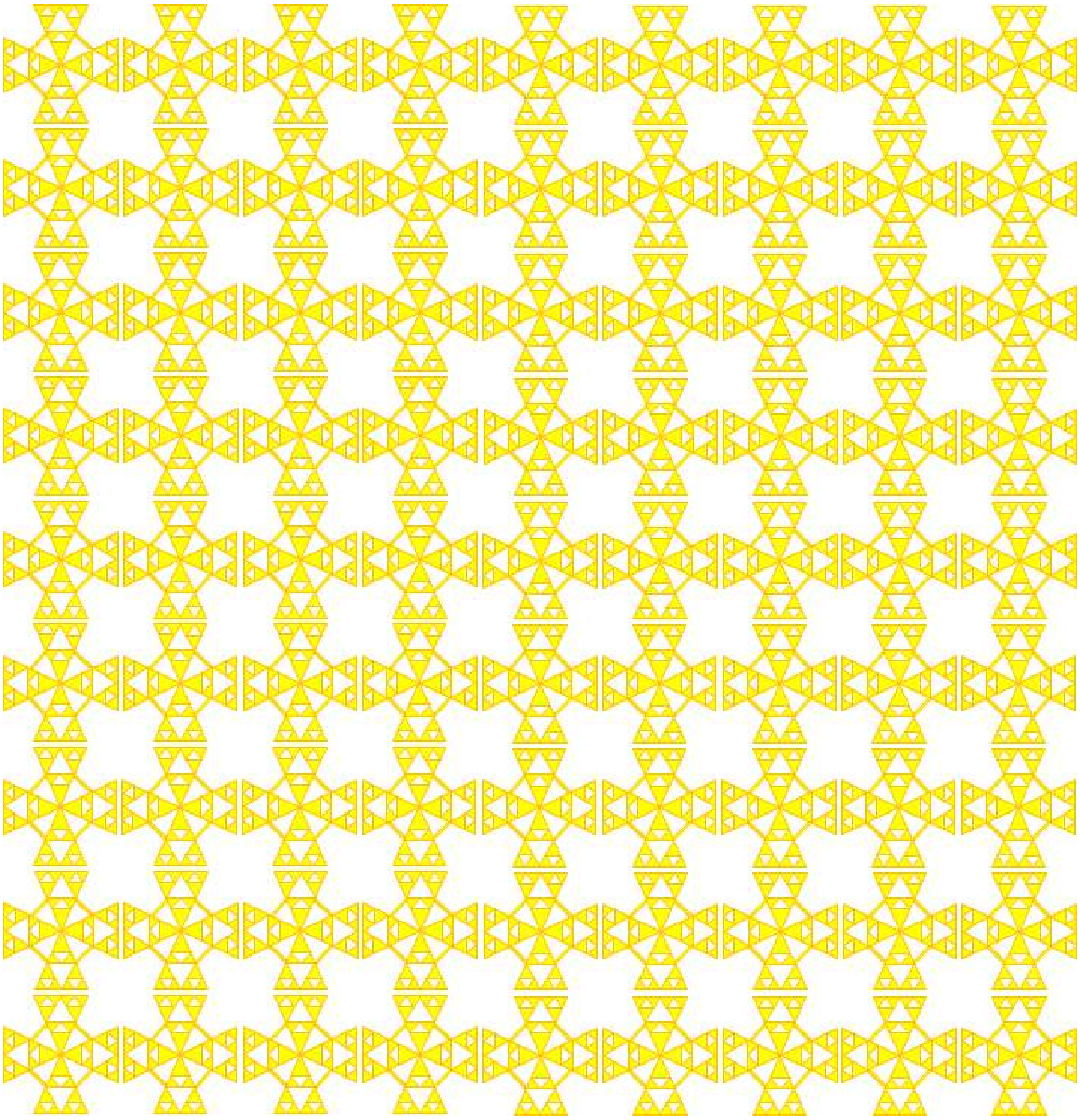

Figure 3.4: The Result of IRS Array Based on the Proposed Unit Cell from CST MWS.

3.3 PERFORMANCE STUDY

3.3.1 Single IRS Results

Figure 3.5 illustrates the S11 (Reflection Diagram) curve for the single element. The solver was configured to display just the points below -10dB, indicating the bandwidth. The parameters are calculated according to the channel performance that was discussed previously.

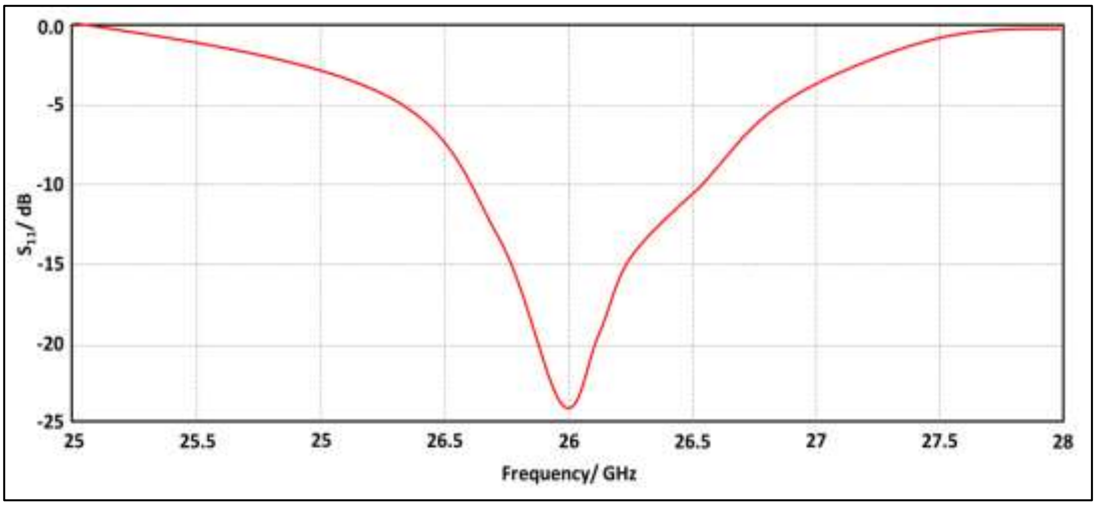

Figure 3.5: S11 Curve of Single Element from CSTMWS.

It can be seen that the bandwidth ranges from 25 GHz to 27 GHz with center frequency 26 GHz. The Farfield single element radiation pattern of the is demonstrated in Fig. 3.6.

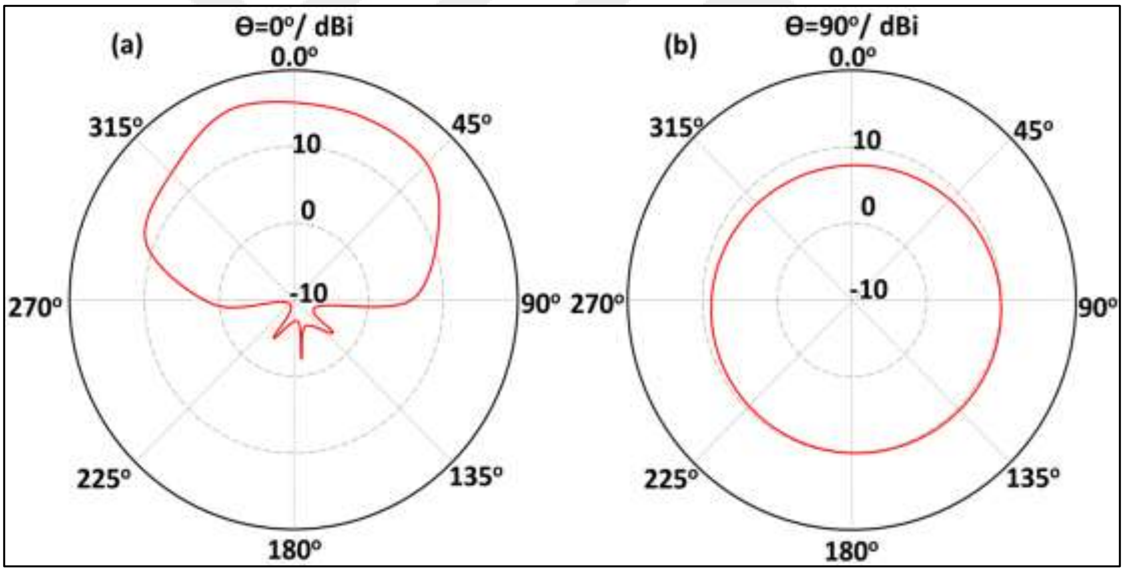

Figure 3.6: Farfield Pattern 2D at f=26 from CST MWS.

The primary lobe direction is at 0.0 degrees. The primary lobe magnitude is 6.94 dBi, representing the gain according to IEEE standards. The proposed antenna gain variation across frequencies are shown in Fig. 3.7.

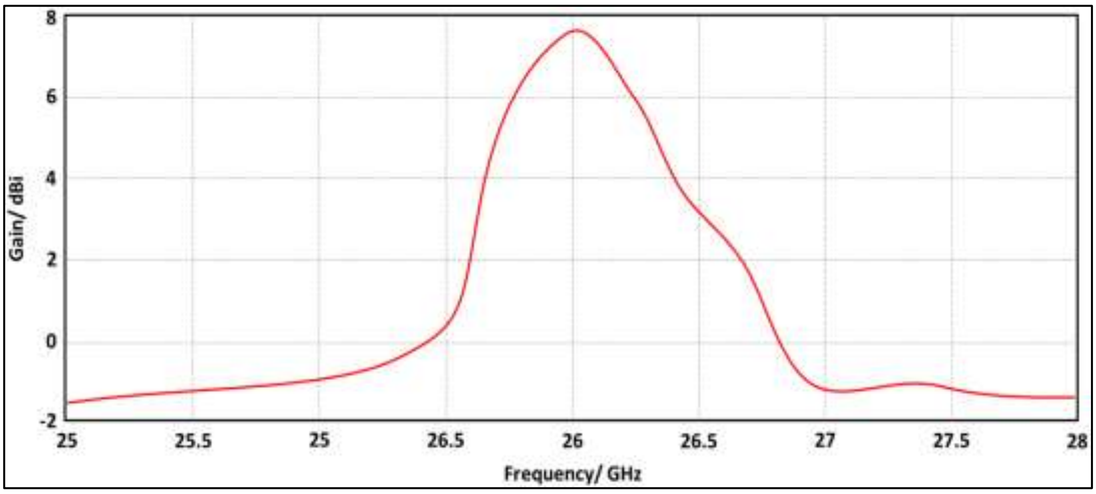

Figure 3.7: Gain Variation over Frequencies from CST MWS.

3.3.2 Array Results

The entire array was tested one element at a time, and the output was summed to get a total from all of the individual array elements. The array Farfield radiation pattern produced by the simulation at the frequency of 26GHz is depicted in Figure 3.8(a) and demonstrates much directional gain with a value of 41.6dBi. Since the phase shift was set to 0°, the subsequent results indicate that the main lobe of gain will continue to be pointing in the 0° azimuth direction as showed in Figure 3.8(b).

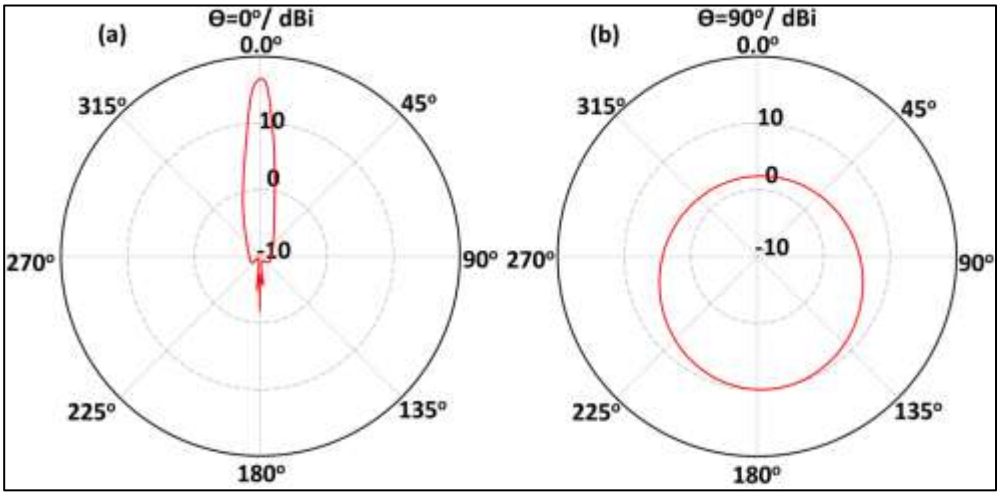

Figure 3.8: Antenna Array Farfield at f=26 GHz from CST MWS.

In order to create the antenna with optimal performance characteristics, the results will be confirmed using CST and HFSS via numerical methods. The S11 and Gain spectrums resulting from the proposed antenna were compared to the results from the above-mentioned software packages. The results presented in Fig. 3.9 indicate an excellent agreement between the two software packages and the results obtained from the antenna design. The proposed antenna shows a gain of 22dBi over the frequency band between 18GHz to 40GHz with excellent matching below -10dB. It is found from the measurements that the effects of rain between 20GHz to30GHz can be reduced when the antenna terminal can change the frequency carrier smoothly during the operation; that will be discussed later. Such frequency bandwidth is achieved by introducing slot array on the antenna cone that matches the electro-magnetic radiation ultimately to the free space impedance with excellent suppressing to the surface waves that reduces the frequency bandwidth [18]. Nevertheless, the antenna directivity is increased rapidly with introducing the reflector that suppress the side lobes significantly [29].

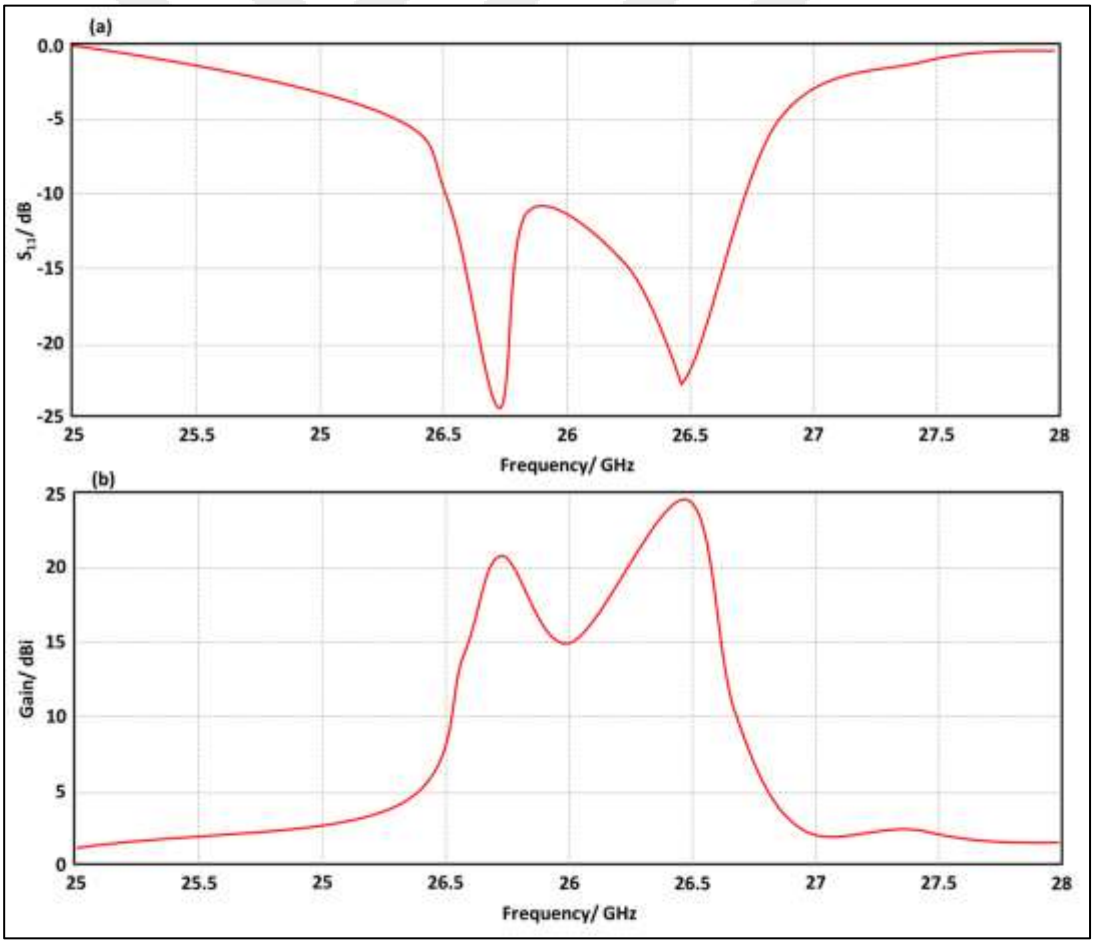

Figure 3.9: The Evaluated Antenna Performance Based on S11 and Gain Spectra from CST MWS.

The suggested antenna exhibits an exceptional gain-bandwidth product attributed to the tangential traveling phenomena elucidated in [3]. Figure 3.10 illustrates the antenna radiation patterns and current distributions. The antenna radiation patterns at 26 GHz and 28.5 GHz are assessed in three-dimensional form. The antenna exhibits an end-fire radiation pattern due to the influence of the antenna's IRS, which achieves high normalization in the E-plane, as discussed in [1].

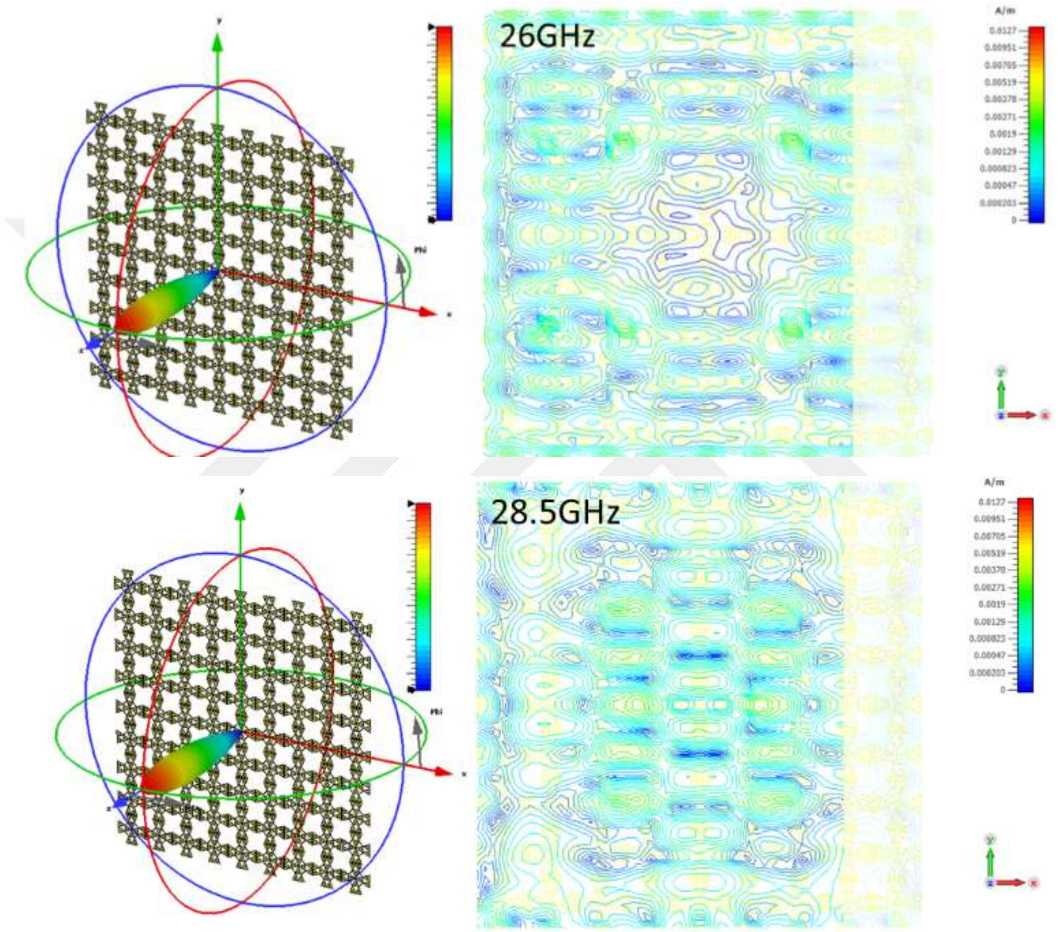

Figure 3.10: Attenuation Using 5G Prediction Models from CST MWS For (A) Lower Operating Frequency of 26Ghz (B) Higher Operating Frequency of 28.5Ghz.

4. DESIGN AND EVALUATION

Programmable EM wave manipulation through the use of arrays of tunable unit cells is being used as a paradigm shift in the creation of wireless environments with Reconfigurable Intelligent Surfaces (RIS). RIS can be low cost and low power user substitutes for traditional active relay and phased array systems and are thus viewed as a key enabling technology for 5G, 6G, and IoT systems. The ability to increase the coverage area, spectral efficiency, and energy efficiency that RIS has generated a large amount of interest from both industry and academia. LDR/PIN/Varactor-diodes based switching and programmable metasurfaces served as the foundation for the earliest RIS prototypes [4-6]. They demonstrated rudimentary reflection control. Although these implementations performed well, they frequently suffered from increased insertion loss and complex hardware issues. More sophisticated versions introduced metamaterial-inspired surfaces and the capability to steer and regulate a beam's polarization by altering its phase [7, 8]. Concurrently, foundational research establishes the theoretical boundaries, realistic models, and design guidelines for RIS-based wireless systems [9–12]. For example, in [3], the authors measured the degree to which RISs outperform de-code-and-forward relays, and in [11], they created practical phase-shift models for RIS beamforming in the real world. Issues with robustness and security in RIS-assisted communication have been investigated concurrently. The authors of [13] and [14] looked into RIS applications for multi-user MIMO optimization and physical layer security, respectively. Additionally, AI has grown in significance. For instance, beamforming, channel estimation, and adaptive optimization of RIS-assisted systems have all made use of deep learning and reinforcement learning approaches [15] and [16]. Comprehensive summaries are provided by recent surveys and tutorials [8, 9], and 18 that highlight the capabilities of AI-enabled RISs to achieve real-time adaptability in dynamic environments. Despite these advancements, certain significant issues remain. The majority of cutting-edge RIS designs either rely on complex biasing networks [4,5], require a lot of space [7], or only concentrate on EM characterization without testing the entire system using communication performance metrics like bit error rate (BER) and channel capacity (CC). Furthermore, even though RIS-enabled compact designs have been reported [7,19], hardware simplicity and support for circular polarization are frequently left out. The need for integrated RIS-assisted antenna designs that balance compactness, re-configurability, and communication-level benchmarks is highlighted by recent research on energy efficiency

[19] and security [20]. Subsequent studies have employed prototypes to concentrate on particular capabilities. While authors in [20] utilized ML to identify anomalies in RF biosensors, authors in [21] employed genetic algorithms to enhance rectenna designs for hybrid energy harvesting. Significant advancements were made in [22]– [24] in the creation of 5G antennae utilizing slotted, parasitic, tapered slot, and reconfigurable fractal designs. Graphene-based metasurfaces for optical beam steering were studied by the authors in [25]. Ku-band CRLH MTMs were examined for V2X applications in [25]. For 5G applications, a wide-band amplifying RIS design was suggested in [27]. Within the RIS-specific domain, the authors of [28] presented a thorough prototype and experimental validation of RIS-based wireless systems. The topic of dual-band shared-aperture systems with autonomous control for mmWave and sub-6 GHz bands was investigated in [29]. Reconfigurable antennae with beam steering and beamwidth adjustment were introduced in [30], enabling adaptive coverage in dynamic wireless settings. Despite these advancements, there are still many problems with the literature as it is now. Many systems either concentrate on constrained bandwidths, do not allow users to precisely modify beam steering angles, or do not vary communication parameters like BER and CC very significantly. Theoretically, RIS is a novel technology for 5G, 6G, and later. They let into manipulate the propagation of electromagnetic waves through materials smaller than a wavelength, whether they are passive or semi-active [31]. RIS may alter the direction, focus, or dispersion of incoming waves to increase coverage, reduce energy consumption, and strengthen the physical layer [32]. Large planar arrays and millimeter-wave bands were the main focus of early solutions, which frequently employed varactor diodes or PIN switches to alter the reflection phase [33]. In order to accommodate low-band 5G and long-range IoT applications, recent research has expanded RIS ideas to sub-GHz operation. Improvements in adaptive beamforming and hardware-implemented MIMO for 5G/6G systems are highlighted in the study [32]. Fast, low-latency phase control over large bandwidths is achieved by means of hybrid analog-digital precoding, programmable RF front-ends, switched-line phase shifters, and DDS-PLL beam-steering architectures. By offering real-time beam updates or initial steering vectors, these solutions can support AI-based strategies and offer deterministic control of radiation patterns [33]. To achieve complete MIMO capabilities in next-generation wireless networks, the suggested RIS unit cell can be combined with well-known adaptive beamforming technology and AI-driven controllers.

4.1 ANTENNA DESIGN AND GEOMETRICAL DETAILS

As shown in Fig. 4.1, the suggested antenna design enhances beams routing and directivity in contemporary wireless communication schemes by combining a dual-layer RIS with a truncated antenna rectangular patch. While middle slots alter the surface current distribution and a centrally positioned cross-shaped slot fine-tunes the axial ratio response, corner truncations introduce orthogonal current components. The radiating element has undergone significant alterations to maximize circular polarization and band-width performance, despite being built on a conventional rectangular microstrip patch. The FR4 substrate to which the patch is affixed has a tan δ=0.02 loss tangent, a relative permittivity of 4.4, and a thickness of 1.6 mm. To reduce back lobes and maintain the same radiation patterns, a complete copper ground plane is etched on the substrate's bottom. Beam steering and directivity are much improved by the suggested RIS structure, which is positioned 1 mm above the patch and eliminates the need for intricate active phase shifters. On a single FR4 base, the two layers of the RIS are mechanically aligned. The top layer consists of concentric square metal structures, while the bottom layer consists of split-ring resonators (SRRs) enclosed in a square framework. There are two LDR switches on each SRR. By altering the SRRs' reaction to variations in light, these switches alter the reflection phase. An inexpensive, impartial, and EMI-resistant form of control is this optically controlled switching technique. It resolves issues with varactor-based RIS systems and standard PIN diodes. The proposed antenna uses different corner truncations to create two orthogonal modes that make circular polarization possible. When the beam is steered, this increases the gain by more than 90%. At the same SNR, using RIS-based beam steering lowers the BER from 1×10^{-2} to less than 1×10^{-4}. This makes the system less likely to make mistakes. When the bandwidth and SNR are the same, MATLAB simulations show that beam steering improves effective CC by almost 25%. Instead of low-loss laminates expensive or complicated stacking multi-substrate, the design uses cheap FR4. This makes it smaller, increases the impedance bandwidth, improves the realized gain, and makes the axial ratio more stable while steering.

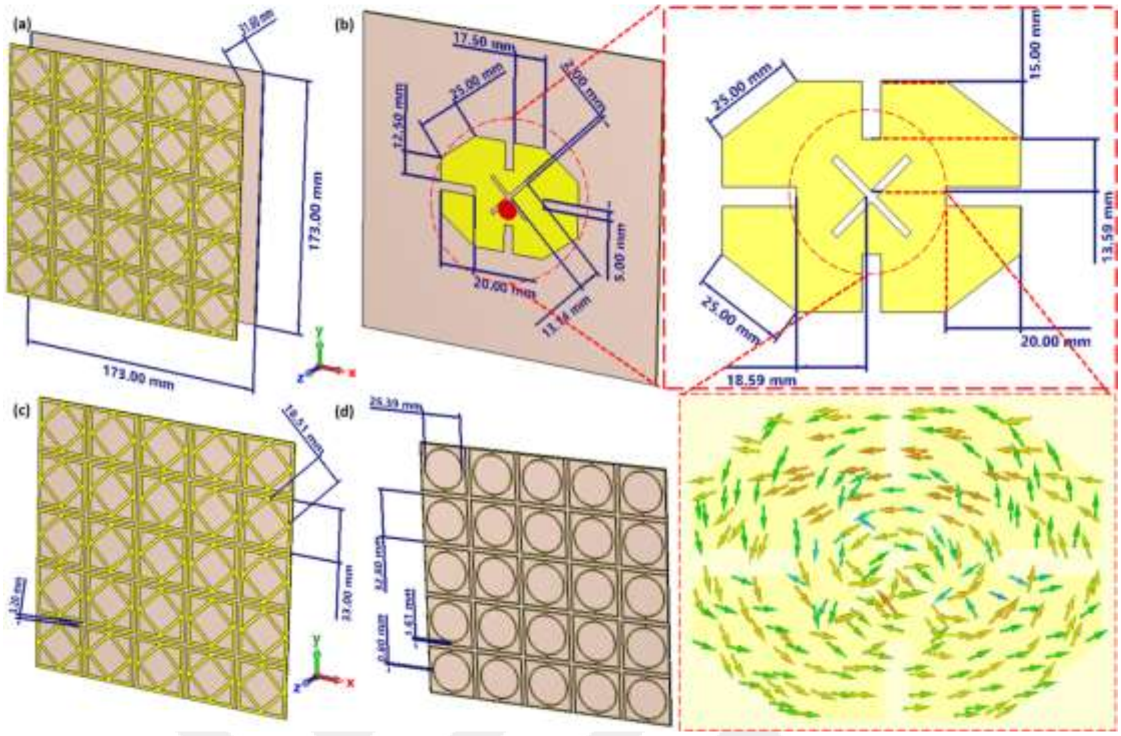

Figure 4.1: Shape of the Antenna Proposed: (A) 3D View, (B) Antenna View Patch, (C) RIS View Front, and (D) RIS View Back.

4.2 DESIGN METHODOLOGY

This paper provides a quantitative performance evaluation with respect to S11 and gain spectra and focuses on antenna design utilizing parametric analysis. The findings show that by adjusting specific parameters, the antenna's efficiency and directivity may be significantly raised. Future studies will look into incorporating novel materials to further improve performance parameters. The proposed antenna clarifies the interactions and polarization of different modes by means of numerical parametric optimization instead of a closed-form analytical framework. In addition to offering a more sophisticated knowledge of the antenna's behavior under different conditions, this approach paves the way for innovative designs that leverage state-of-the-art computational techniques. Researchers intend to improve antenna technology and make it more flexible to meet evolving communication needs by employing this strategy. Because of the metasurface layer and the many corner truncations on either side, the electromagnetic environment is closely connected. We calculated the initial patch sizes using a typical microstrip-cavity approximation. We conducted a thorough parametric sweep in three dimensions to identify the combination that would preserve the highest efficiency while achieving the required 90-degree modal phase shift for circular polarization. This approach allowed us to identify the optimal patch sizes and shapes, ensuring that the necessary performance requirements were met. Additionally, we might improve our design to increase bandwidth and reduce losses by examining the interaction between the metasurface and the underlying substrates. Our models' findings demonstrated notable gains in bandwidth and efficiency, demonstrating the efficacy of our design changes. We intend to build prototypes and carry out experimental validations as a further stage to evaluate the MTS usefulness in actual applications.

4.2.1 Antenna Performance without RIS Inclusions

The author directed the improvement of patch performance to satisfy predetermined requirements by carelessly examining the antenna project, a suggested RIS layer. In order to improve the general functionality, the team put creative solutions to the problems found during the evaluation and worked hard to resolve them. The project thus started to pick up steam, drawing interest from a range of stakeholders who were keen to see the developments come to fruition. In the first scenario, the author employed a rectangular patch; in the second, truncation etching was done at the patch's corners; in the third, slots were added to the antenna patch; and in the fourth, cross lines were incorporated. Every variant sought to improve the antenna's bandwidth and efficiency while offering vital information for upcoming designs. Significant gains in performance indicators were shown by the results, which encouraged more research into cutting-edge materials and designs. Figure 4.2, which displays shapes four of structural alterations intended to isolate distinct electromagnetic effects, includes images of each scenario. These results confirm the original theories and pave the way for further antenna technology research. In order to get better performance gains, future research will focus on improving these setups. Case 1 creates the basic resonance TM10 around 0.915GHz, Case 2 perturbs the TM01 mode with single-corner truncation, Case 3 achieves the 90° phase shift with unequal multiple truncations, and Case 4 adds a layer metasurface and optimization feed to increase gain and widen the axial-ratio impedance bandwidth. These modifications demonstrate the complicated relationship between design alterations and their impact on electromagnetic performance. By analyzing each case, we can better understand how specific changes contribute to the overall efficiency and effectiveness of the system.

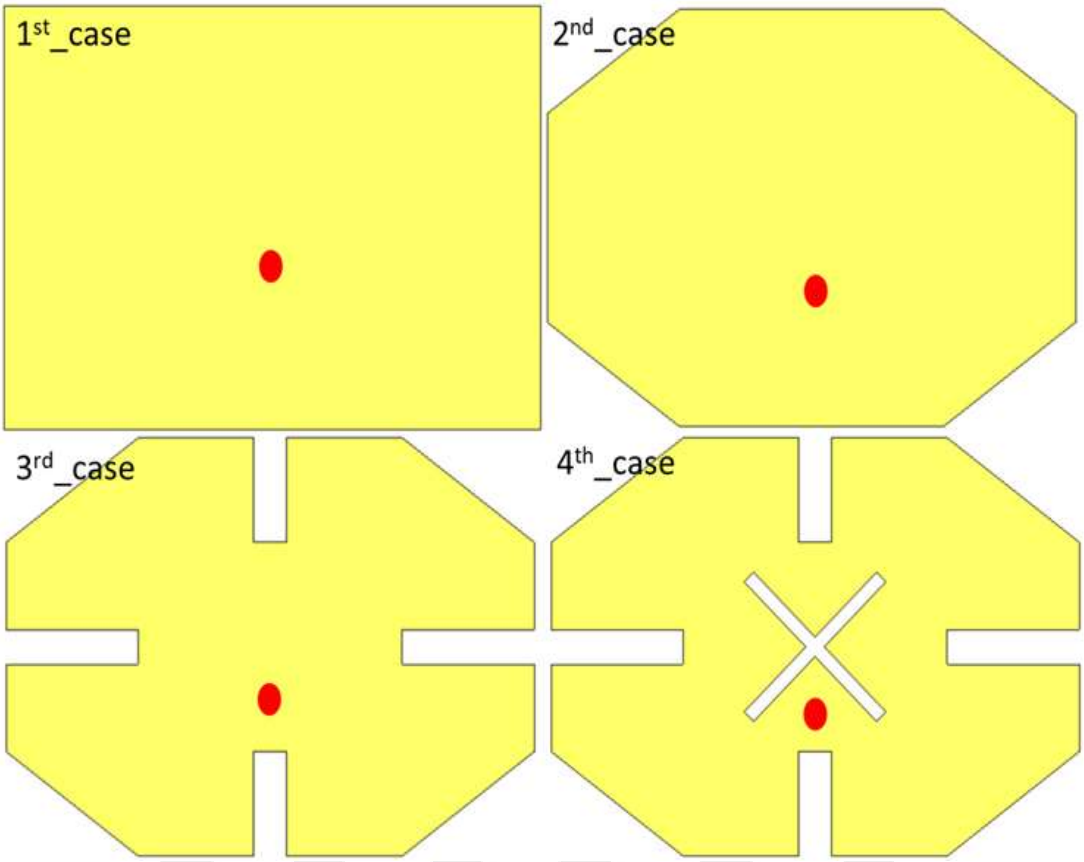

Figure 4.2: The Considered Cases.

The antenna that was based on the fourth scenario performed at its best in terms of gain, polarization, and bandwidth. With outstanding circular polarization below -3dBi and gain above 5dBi, it had a bandwidth of 0.9GHz to 2.7GHz. As seen in Fig. 4.3, another frequency range included frequencies from 3.2GHz to 3.6GHz with a gain of about 5.5dBi and no achievement of circular polarization. The radiating structure's sequential evolution is what caused the antenna's performance to increase. The basic TM10 mode is supported by the first rectangular patch, which offers linear polarization with a small impedance bandwidth. The TM01 mode is lowered to pair with about identical magnitude and a 90° phase difference as a result of unequal corner truncations, which also increase the matched band and provide circular polarization. The impedance bandwidth is increased and the overall quality factor is decreased by inserting slot a narrow along the diagonal patch. To stabilize the broadside gain pattern and shape the radiation aperture, a thin parasitic strip is introduced. According to full-wave simulations, every stage results in a discernible improvement; for example, slot insertion increases the bandwidth impedance by 12%, feed optimized with partial ground extends the bandwidth by 6%, and uneven corner cuts raise the bandwidth by 40%.

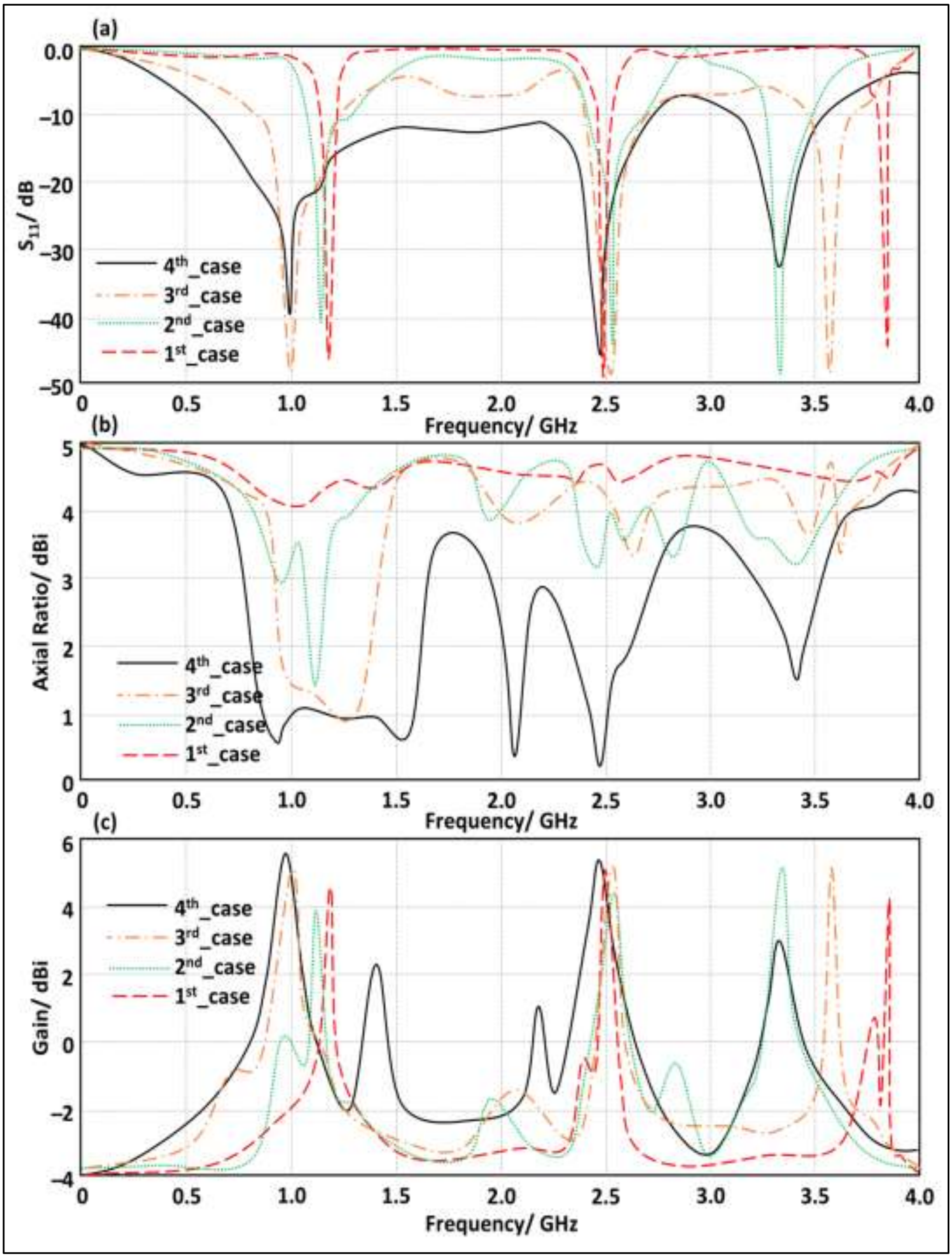

Figure 4.3: Simulated Results of the Antenna Without RIS Layer: (A) S11 Spectra, (B) Polarization Spectra, and (C) Gain Spectra.

4.2.2 RIS Design

The integration of two types of structures, specifically the combination of a patch and a plane ground, creates a new RIS Unit Cell design with increased performance characteristics. The unit cell is branded by obtaining the relative permittivity from S-parameter results from simulation. The effective permittivity of the unit cell was obtained from the electromagnetic simulation model using an infinite array of duplicates of the unit cell. The boundary conditions used in the simulation were perfect magnetic conductor in the z-direction and perfect electric conductor in the x-direction [16]-[17]. The description of the electromagnetic characteristics of the unit cell is performed using mode Floquet analysis via CST Microwave Studio. In addition to determining the characteristics of the unit cell's electromagnetic characteristics, the model produces an infinite periodic array of the unit cell. The model outputs fundamental data, such as the refractive index, the modes of propagation, the phase and amplitude of transmission and reflection. This information is critical to improving the unit cell's dynamic tuning and resonant operations. Finally, a separate full- simulation wave of the overall finite geometry demonstrates the efficacy of the antenna system comprised of the full 5x5 RIS finite array combined with the excited patch antenna and a finite feed port ground plane and SMA.

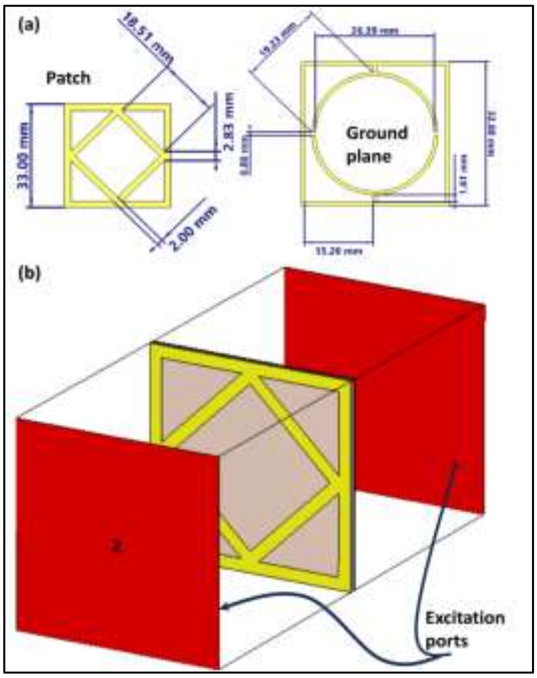

Figure 4.4: The Proposed Unit Cell of the Proposed RIS: (A) Unit Cell Details and (B) Waveguide Analysis.

The concepts of near-field reactive coupling and structured electromagnetic resonance have been used to develop the suggested antenna design. The technology makes advantage of RIS, an energy-losing driven Fabry-Pérot cavity [14]. This novel strategy seeks to improve signal efficiency and quality, which could result in improvements in wireless communications. By increasing the efficiency of energy transfer within the cavity, the design has the potential to enhance significantly the performance of next-generation antenna systems. The RIS is made up of two layers of metal: a patch with a pattern on it and a ground plane that is always there. The dielectric substrate is held in place by these layers' creation of boundaries that only partially reflect. Two distinct resonance frequencies are produced by the design: 0.915 GHz and 2.05 GHz (for further details, refer to Fig. 4.5(a). The structure's effective capacitance and inductance are altered by the top patch's form. The resonant qualities of the structure are attributed to this feature. Because these resonances cause significant changes in the input impedance, the conjugate can be aligned with the open space within a narrow bandwidth, which reduces reflection. This characteristic enables the optimal coupling of incident energy cavity into modes. The peaks in the parameter transmission S12 in Figure 4.5(b) indicate that the energy is subsequently re-radiated. Additionally, large decreases in S12 indicate the presence of a bandgap electromagnetic, which reduces the amount of parasitic surface wave modes that could impair the antenna's performance and prevents surface waves from propagating. The beam is produced by the real-time phase shift of the RIS unit cells made possible by the dual-band resonance. This feature improves the antenna system's overall efficiency by providing more exact control over the radiated beams' form and direction. Therefore, wireless communication systems and other applications that need dynamic beamforming may see major gains as a result of the integration of cutting-edge RIS technology.

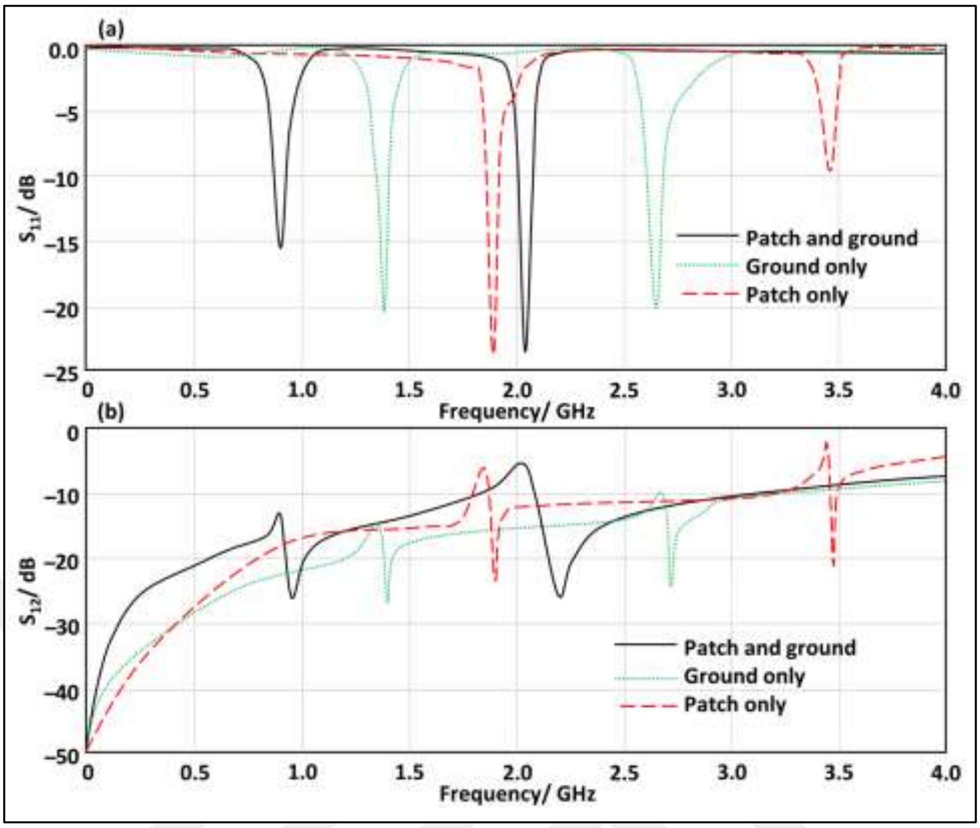

Figure 4.5: The S-Parameters of the Proposed Evaluated RIS Cell Unit: (A) S11 and (B) S12.

The suggested RIS unit cell responds differently to electromagnetic radiation depending on the LDR switching states, which are 00, 01, and 11. By altering the RIS's impedance, these switches modify the way signals are sent and reflected. The resonant frequencies shift and the depth of the reflection decreases as it exchanges states. This process is always carried out. Eleven states, for example, shift nulls due to their increased electrical connectivity. Equally, the 00 state exhibits profound nulls at specific frequencies, representative that resonant modes are significantly influencing one another. The amount of transmission loss is altered by diode biasing. High-impedance gaps prevent some modes of transmission, whereas lower junction resistance facilitates coupling. By demonstrating how variations in the boundary circumstances alter the deliveries of fields electric and magnetic, which alters the energy balance, Maxwell's equations may be able to assist us comprehend these phenomena. The excitation of these modes may be affected by the MTS ability to support a variety of resonant modes, including magnetic and electric dipolar modes. The proposed RIS reconfigurability is controlled by optically-controlled switches using light-dependent resistors (LDRs), which function as variable resistors set by external illumination. This regulated spectral behavior allows the unit cell to function adaptively across several frequency bands or to obstruct unwanted interference in RIS applications (see to Fig. 4.6). LDRs generate an additional resonant state with an independent reflection phase upon illumination, hence closing SRR gaps.

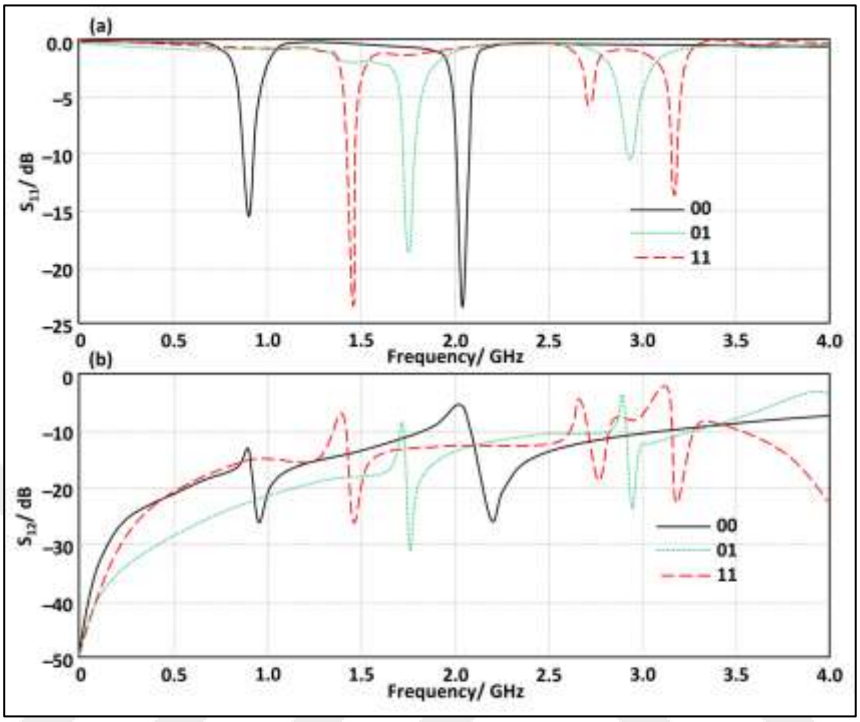

Figure 4.6: The Proposed S-Parameters of the Evaluated RIS Cell Unit Different with Switching Shapes: (A) S11 and (B) S12.

4.2.3 RIS Effects

The RIS Layers have a significant effect on the gain of 0.915 GHz on 16.8 dBi and can be seen in figure 4.7, which is due to the combination of near-field coupling and the theory of classical electromagnetic aperture. The RIS Layers are made from factory industrial; substitute-wavelength sized unit cells. The unit cell with varying reflection phase across space will change the phase front of the incoming field from the antenna. The RIS produces a coherent beamforming effect at 20 mm of distance to the antenna, implying that the combination of the fields directly radiated and the reflected fields yield a strong resultant field in the desired direction. As a reactive element, it modifies the electromagnetic field conditions, both electric and magnetic, at the edge of the elements. This increases the aperture function without introducing additional moving parts. The reflection phase of the RIS is symmetric with respect to the antenna's polarization, as shown by the Spectrum of the Axial Ratio. This indicates a constant amplitude and relative phase. The optimal spacing is related to the increase of the Fresnel region phase. The RIS modifies the phase front of the Wavefront in a similar manner to that of a Lens. It therefore causes the wavefront to be more concentrated to have a smaller beamwidth and to be directed more narrowly, thus producing a direct result of the energy output.

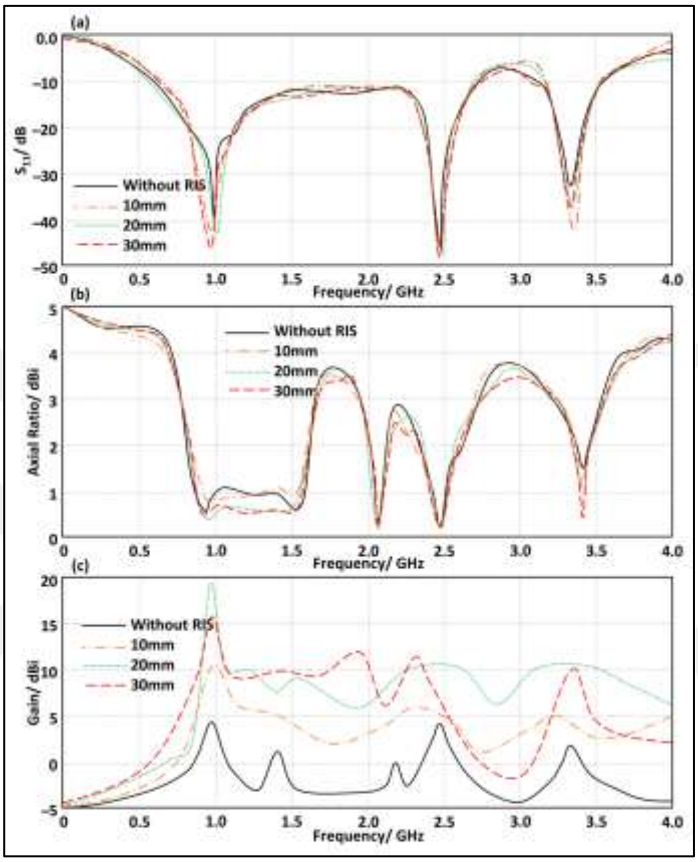

Figure 4.7: Results Simulated of the with RIS Layer Antenna: (A) S11, (B) Polarization, and (C) Gain.

As demonstrated in Figure 4.8, the lobe of maximum intensity can be controlled from a maximum at an angle of +22 ° to a maximum at an angle of -22° (Fig 4.8) by turning on the Load LDR of the proposed Reflective Intelligent Surface (RIS). This complex behavior can be attributed to the control of electrodynamic phase gradient and the array theory. Based on how the LDR has been configured, the unit cells of the RIS will provide a different set of reflection phase shifts. Thus, the RIS behaves like a passive phased array. Furthermore, as the LDR switching shapes vary, the effective surface impedance of the proposed unit cell is also changing dynamically. As a result, the local reflection phase φ (x, y) is being modified throughout the planned RIS, in turn allowing into form a phase distribution at the aperture of the RIS. The combined effects of the reflection phase shifts are effectively added together as a Fourier Transformation creating the Farfield radiation pattern from each aperture location. When it improves a uniform gradient of reflection phase distribution to the entire RIS surface, then the transverse wave vector direction of the primary beam will change as per Snell's law:

$$\sin \theta_r = \sin \theta_i + \frac{\lambda}{2\pi}\frac{d\emptyset}{dx} \quad (4.1)$$

The phase gradient from switching LDR states is represented by the variables dx and dϕ in the equation under discussion. A positive gradient points the beam in one direction (+22°), whereas an inverted gradient points it in the opposite direction (-22°). This behavior is similar to phased antenna arrays, which change the direction of the beam by varying the excitation phase of each element. Reactive loading and resonance states within each cell are passively influenced by changing the reflection phase with LDR switching in the suggested RIS scenario. Modifying the amount of energy stored and released will alter the phase of the re-emitted wavefront. The aperture's actual size and the RIS components' phase swing capabilities determine the steering range. This permits a measured steering range of ±22° and about 360° phase control. The amplitude response of the RIS remains constant despite variations in the phase gradient. This prevents distortion or loss of gain in the steering. By improving directionality and gain, this improves smart beamforming in communication systems. As the suggested MTS-based antenna links to the patch radiator, its loading is reflected in the gain fluctuation. A high-impedance surface is produced by this two-dimensional periodic array of subwavelength unit cells. The surface impedance transitions from inductive to capacitive at resonance at 0.915 GHz, reaching a peak realized gain of roughly 16.8 dBi with a supplement loss of less than 0.2 dBi but the reflection phase diverges away from resonance, which lessens constructive interference. The computed surface-wave suppression is consistent with the observed ±0.5 dB gain difference.

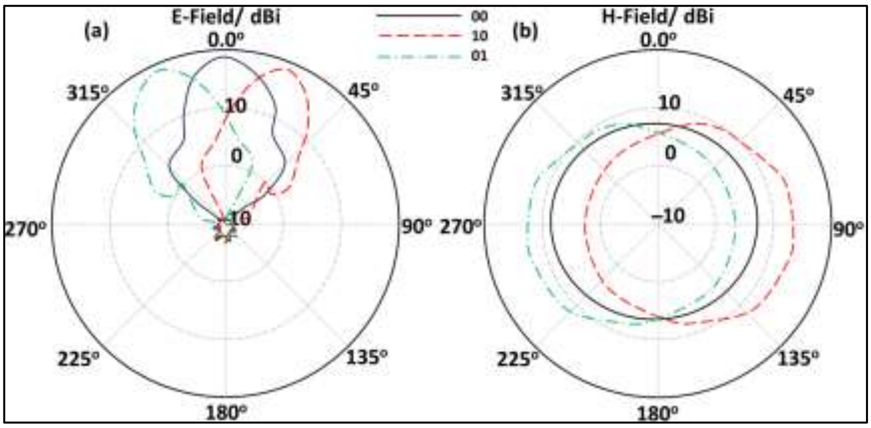

Figure 4.8: The Antenna Radiation Evaluated Patterns on the RIS Based Layer with Different Shape Process: (A) E-Plane and (B) H-Plane.

4.3 EXPERIMENTAL REALIZATIONS AND MEASUREMENTS

As shown in Fig. 4.9, the suggested antenna is made in this section utilizing a chemical wet etching procedure. The antenna prototype is made using the conventional photolithography process, as seen in Fig. 4.9. Fig. 9(a) displays the patch antenna portion under consideration. Fig. 9(b) shows the complete antenna setup based on the suggested study. In Fig. 9(c), the suggested RIS is on display. S11 and radiation pattern tests are performed on the suggested antenna. LibreVNA 2 ports complete VNA 100kHz - 6GHz Network Analyzer (VNA) is used to measure S11 outcomes. Inside an RF chamber, a dual polarized horn antenna (LB-SJ-20180), signal generator a N9030A PXA signal analyzer, and a are used to detect the radiation patterns.

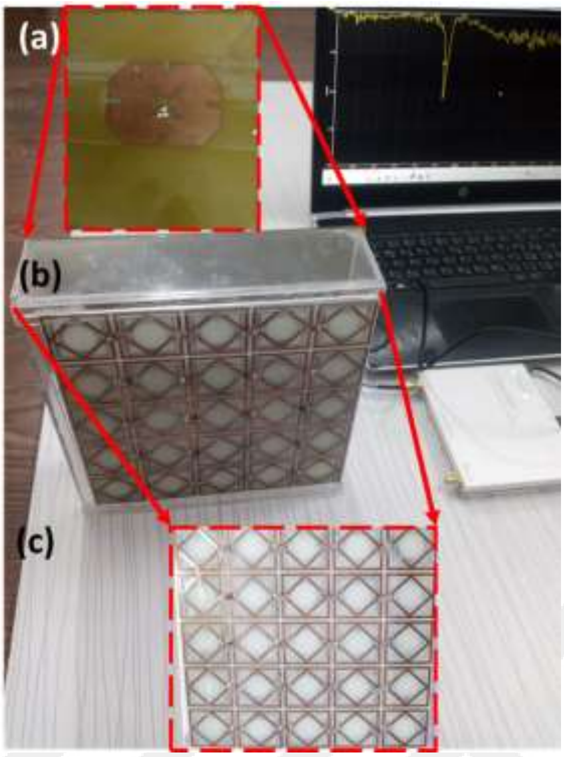

Figure 4.9: The Fabricated Prototype Antenna: (A) The Antenna Considered Patch, (B) The Structure Antenna and (C) The RIS Proposed.

4.3.1 Antenna Validation Performance

An integrated antenna and RIS system are exposed in Figure 10, which provides a much larger overall operating bandwidth than what would usually be considered optimal, and thus [would be on average] more ideal to use as a means for both manual and automated communications. Although the final measurements of the integrated RIS system were taken at the center frequency of the band operating, the numerical results of CST MWS and experimental validation show excellent agreement for frequencies both below and above the center frequency, thus giving an idea of where a majority of the losses occur when transferring energy through this structure. The broader area with many resonance points creates a wide, continuous bandwidth of operation, over which the antenna-RIS system will generate constructive interference with beams directed toward a specified direction. Thus, the RIS element of the integrated antenna absorbs the aperture field created by additional lobes of the antenna and directs the combined aperture field to create a main lobe, as measured in the far-field of the radiation pattern for this design. Furthermore, the antennae constructed with RIS elements measure the change in phase of the waves, due to frequency, and allow for continued efficacious collimation of the wavefront for many incidence angles. The operation of the RIS is similar to a phased array antenna, but it uses a multitude of different movable reactive loads instead of multiple active phase-shifting devices to create a constructive interference pattern. Overall, the results of the experiment validated the initial theoretical models, indicating that this type of design would be applicable for any type of intelligent wireless communication systems requiring beam steering for a variety of different frequencies. The testing also revealed that the proposed antenna can successfully steer beams as far as -22 to +22 degrees. This is accomplished by swapping the LDR devices' states from 00 to 01 to 10, as illustrated in Fig. 4.10.

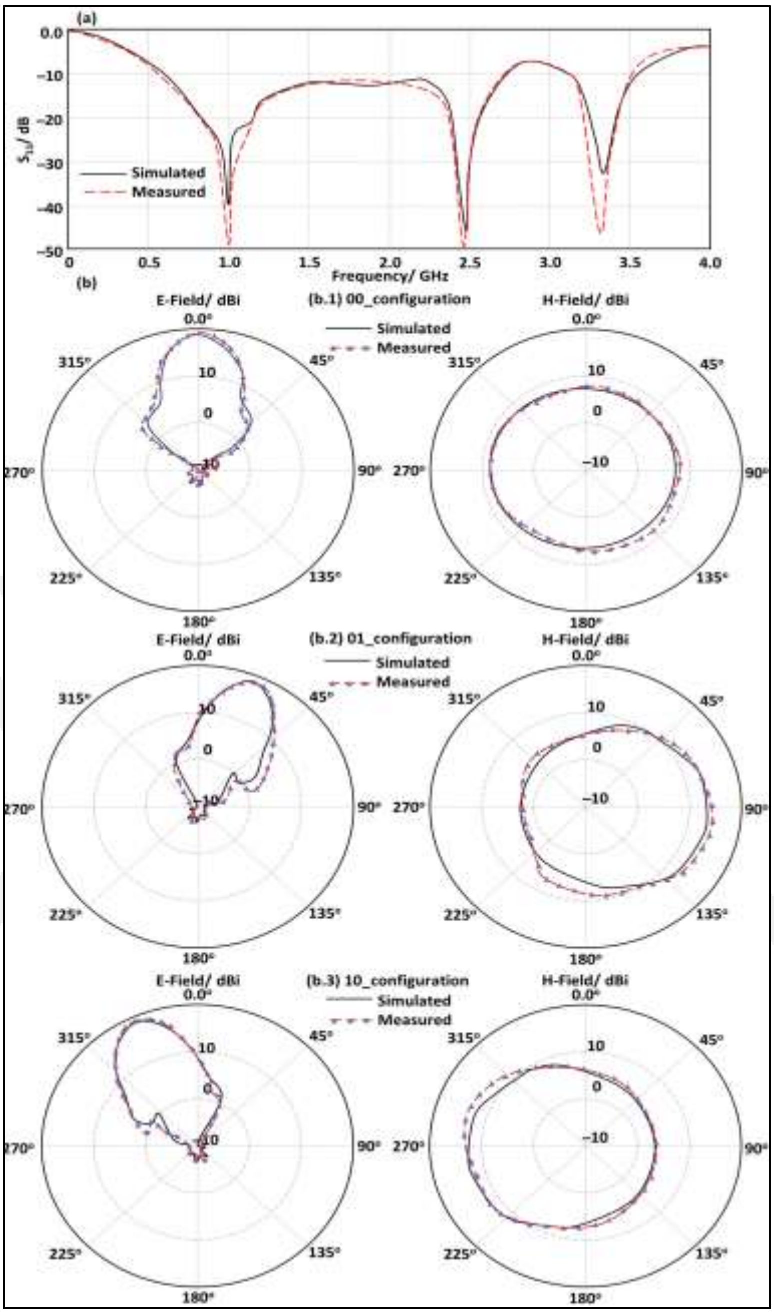

Figure 4.10: Antenna Results Validation: (A) Spectrum S11 and (B) Patterns Radiation at 0.915Ghz At Switching Different Shapes. (B.1) The Radiation Antenna Patterns at 00_Shape, (B.2) The Radiation Antenna Patterns At 01_Shape, and (B.3) The Radiation Antenna Patterns at 10_Shape.

The proposed metasurface-loaded patch antenna exhibits effective Circular Polarization (CP) performance throughout its operational Bandwidth. The main lobe of the antenna has a defined broadside direction with a Broadside Beamwidth of approximately 19° at a gain of 3 dB; thereby creating the appearance of having two symmetrical lobes. In addition, the E-Plane and H-Plane Cross-Polarization levels remain consistently 17 or more dB lower than Co-Polarization levels within the main beam. Therefore, this antenna's capabilities for achieving Cross-Polarization Discrimination (XPD) consistently exceed the recommended range (15-20 dB) for high-quality Circularly Polarized Antennae. Hence, the proposed patch antenna design can produce strong right or left hand circularly polarized fields based on the low cross-polarization level. An additional contributing factor for achieving superior CP performance with the proposed antenna design is its capacity to reflect In-Phase at High Impedance. The Completely Eliminated Surface Waves and Increased Electric Field Strength above the Ground Plane permitted the antenna design to promote equalized Amplitude of both TM10 and TM01 modes created from the Non-Symmetrical Patch Design, thereby increasing the Broadside Gain of the antenna system. The result is a reduced constant range of change for the Axial Ratio across the Principal Lobe, providing a much "cleaner" Circularly Polarized Field. The radiation pattern's symmetry, with equal half-power beamwidths and no pattern distortion in either the E-plane or H-plane cuts, is another indication of strong CP behavior. In real life, when the sending and receiving nodes' locations can fluctuate, this consistency is extremely beneficial. In conclusion, the co- and cross-polar patterns that were measured show that the proposed MTS-loaded patch antenna achieves true circular polarization, which meets the strict rations for modern applications and delivers high efficiency radiation and purity polarization, even though direct AR measurement is not possible, as shown in Fig. 4.11.

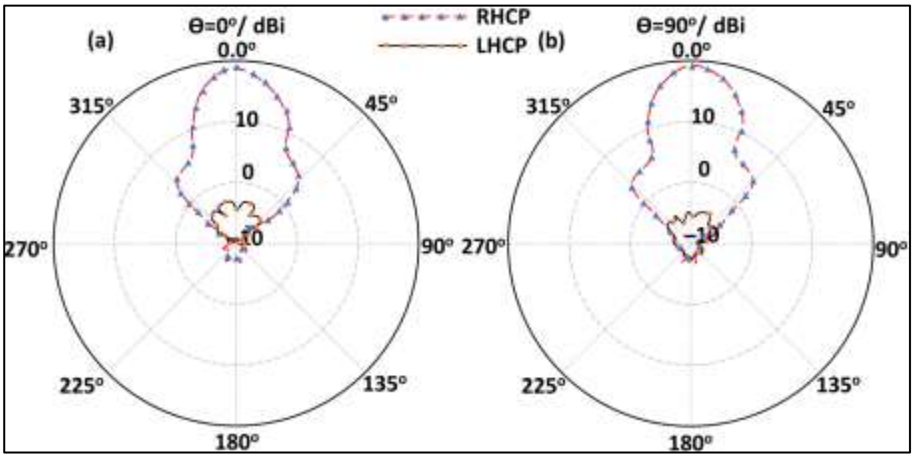

Figure 4.11: Measured Antenna Radiation Patterns at 0.915GHz At Different Polarization and Orientation: (A) E-Plane and (B) H-Plane.

4.4 PERFORMANCE CHANNEL

The recommended RIS that uses LDR switches makes big improvements in beam passive steering, letting it directs effectively over a range of ±22° at 5.8 GHz. The system uses energy well, but it doesn't switch very quickly. Figure 4.12 shows that the best performance happens when the alignment is at 0°. A 15° misalignment, on the other hand, slightly lowers the BER and CC. Table 4.1 shows how this antenna design is different from others that have been shown before. It shows that this design is smaller and works better for applications below 6 GHz, with a gain range of 10.5 dBi to 16.8 dBi over 0.9–3.5 GHz. It is easy to change settings with resistor LDR-based low-dropout topologies, and they keep loss insertion to a minimum.

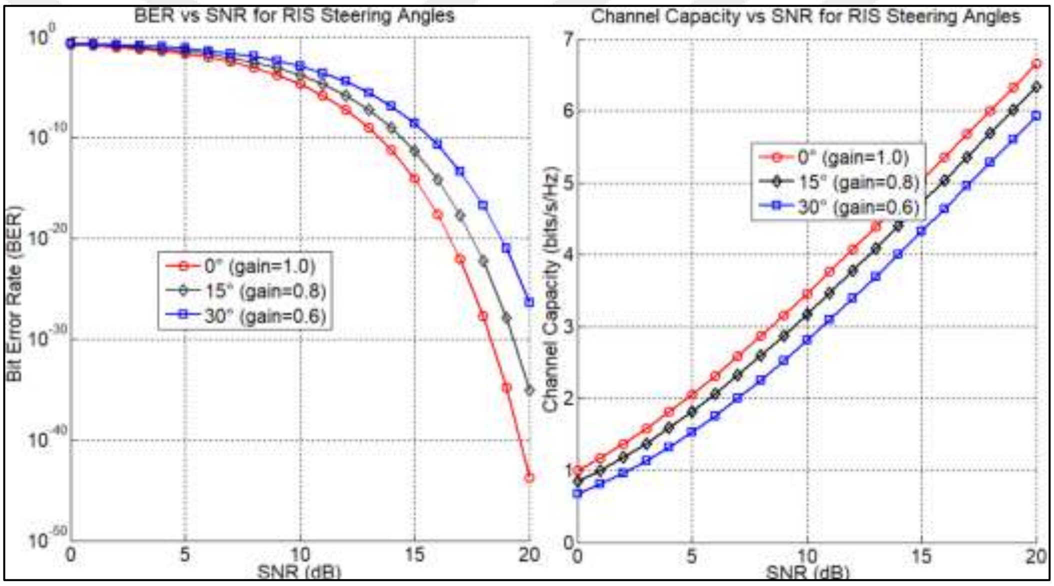

Figure 4.12: The Terms Evaluated in Performance of: (a) BER and (b) CC.

Table 4.1: A Comparison Between the Proposed Study and Other Published Results.

Size/ mm2	Bandwidth (BW)	Gain	Beam Steering Angle	CC Impact	Switching Technique	Ref.
173×173	0.9–3.5 GHz (~2.6 GHz span)	10.5–16.8dBi	±22°	Capacity: ~5.4 bits/s/Hz at 0° steering (16.8dBi), ~4.8 bits/s/Hz at ±22° (10.5dBi); BER < 10?5 at SNR > 15dB	LDR	This Work
800×800	350 MHz (- 1dB BW)	23dBi at 2.3 GHz; 19.1dBi at 28.5 GHz	0–60° (broadside) steering	Not explicitly stated	2-bit phase shifting with PIN diodes	[29]
300×300	22.5–29.5 GHz (26.9% fractional BW)	(Not specified indBi)	±50°	Not quantitated	One-bit PIN switches	[30]
400×400	Dual-band	(Not specified)	±35° (sub-6), ±30° (mmWave)	Not quantitated	RF switches controlling shared aperture	[31]
210×140	~4% BW at 5 GHz	~8dBi	±40° elevation & multi-azimuth	+29% coverage capacity, +16% throughput	PIN diode-controlled pixels	[32]
140×200	Dual-frequency	(Not stated)	10°–45° at 27 GHz & 31 GHz	+50% at 20dB SNR; +84% at 60dB	Varactor tuning via ML biasing	[33]

5. CONCLERUSION AND FUETURE WORCKS

5.1 CONCLERUSION

This work presents a design for a fractal IRS unit cell element intended for application in 5G mm-wave communication systems. The proposed element is a square patch that is 5 mm² in size. The suggested unit cell has a gain of 7 dBi and a bandwidth of 2 GHz centered at 26 GHz. After that, the unique design is made into a 10×10 grid of the same parts on the x-y plane. The array increases the gain to 26 dBi while still keeping the radiation efficiency high. The results show that the proposed IRS array is a good choice for 5G because it is easy to make, smaller than other designs, and works well. Researchers are very interested in how to make IRS that works in the mm-wave frequency band. It's harder to make antennae with slots and shapes because they have to be small for high frequencies. Millimeter waves can pass through walls and other obstructions due to their short wavelength. This makes the signal weaker when there is no direct line of sight. To solve the problems that mm-waves cause, big 5G transmitters and receivers are used. It is much harder, on the other hand, to keep IRS arrays working in these frequency ranges. The main goal of this research project is to design, improve, and test an antenna system that uses RIS and works between 0.9 GHz and 3.5 GHz. The antenna consists of a small antenna and an RIS layer that is controlled by LDR switches. Because of this, the antenna's gain is better, and its container change how it sends out signals. For the best performance, there should be a space of twenty millimeters between the antenna and the RIS. Such an arrangement makes it clear that coupling optimization is very important in systems that use RIS. The gain advantage helps not only the broadside operation, but also the RIS works well at steering angles of ±22°. To effectively guide the beam, it requests to carefully change the LDR biasing settings of the RIS unit cells. The device can control the main beam within a range of ±22° by carefully changing the switching patterns. The experimental validation, which usages VNA capacities for S11 and radiation pattern characterization in an RF chamber, matches up very well with the modeling results that were found using CST Microwave Studio. The circularly polarized antenna that has been shown is supposed to have a high-gain (16.8 dBi), little cross-polarization, and a small beam navigation at 0.915 GHz. These traits make it suitable for many diverse wirelesses uses. Some of the goals for future development are to change the geometry of MTS to give it a wider high-impedance response, such as by adding dual or multi-band operation, improving beam steering, and making things smaller and more integrated for small Internet of Things nodes and unmanned aerial vehicle platforms. This study demonstrates the fabrication of a fractal IRS unit cell element for application in 5G mm-wave communication transmission systems. The part that was discussed looks like a square patch that is 5 millimeters by 5 millimeters. The proposed unit cell has a center frequency of 26 GHz and a gain of 7 dBi. Its bandwidth is 2 GHz. Then, the unique design is turned into a grid of identical parts on the x-y plane, which is 10 by 10. The array keeps a high radiation efficiency while also increasing the gain by raising it to 26 dBi. The results indicate that the IRS array that was shown is a great choice for 5G because it is easy to make, smaller than other designs, and works well. Building an IRS that operates in the mm-wave frequency range is of great interest to researchers. It is harder to make antennae with slots and forms when they have to be small for high frequencies. Millimeter waves can go through anything in their way because their wavelength is so small. This weakens the signal when there is no line-of-sight connection. Big 5G transmitters and receivers are used to address the problems that mm-waves cause. On the other hand, it is much harder to keep IRS arrays working at these frequencies.

5.2 FUTURE WORK

a. Future research may focus on developing intelligent algorithms utilizing deep reinforcement learning (DRL) and federated learning for dynamic adjustments in backscatter devices' power, frequency, and reflection coefficients.

b. These advancements aim to improve efficiency spectral and interference mitigate in extensive 6G areas.

c. Hybrid systems combining reconfigurable intelligent surfaces (RIS) or STAR-RIS with backscatter-assisted NOMA are proposed to improve signal coverage and energy collection.

d. Enhancements in privacy and security require lightweight security frameworks for passive and semi-passive backscatter devices in NOMA systems.

e. Techniques like chaotic mapping, keyless encryption, and secure beamforming are suggested to ensure the integrity of backscattered communications in busy 6G IoT environments.

f. Exploration of new frequency bands for backscatter-NOMA networks, including terahertz (THz) and visible-light communication (VLC), is encouraged due to their high capacity and low latency, suitable for applications like augmented reality, smart healthcare, and IoT in factories.

g. Development of small, high-gain metasurface-based backscatter tags is proposed to efficiently convert radio frequency (RF) to direct current (DC) to enhance hardware prototyping and energy harvesting.

h. Real-world testing of adaptive impedance matching and energy recycling systems aims to connect theoretical models with practical applications in 6G infrastructure.

REFERENCES

[1] G. Al-Gburi, M. Alibakhshikenari, B. S. Virdee, T. M. Hameed, D. Mariyanayagam, S. Fernando, I. Lubangakene, Y. Tang, S. U. Khan, and T. A. Elwi, "Microwave-based breast cancer detection using a high-gain Vivaldi antenna and metasurface neural network approach for medical diagnostics," Frequenz: Journal of RF-Engineering and Telecommunications, 2025. [Online]. Available: (in press).

[2] B. S. Bashar, T. A. Al-Sharify, Z. A. Rhazali, H. Misran, M. M. Ismail, and T. A. Oleiwi, "Miniaturized MTM Antenna for 5.7 GHz Services," 2024 4th International Conference on AI and Signal Processing (AISP), Vijayawada, India, 2024, pp. 1–5, doi: 10.1109/AISP61711.2024.10870668.

[3] B. S. Bashar, B. G. Mejbel, Z. A. Rhazali, H. Misran, M. M. Ismail, and T. A. Oleiwi, "Design of Metasurface Antenna for 5G Applications," 2024 4th International Conference on AI and Signal Processing (AISP), Vijayawada, India, 2024, pp. 1–4, doi: 10.1109/AISP61711.2024.10870657.

[4] R. M. Zaal, N. N. Kamal, M. A. Ahmed, S. H. Ghadeer Al–Sultani, S. K. Bin, and T. A. Oleiwi, "Direct Antenna Beam Squint Correction Using AI-Equalization Strategy for 3D MIMO Array System," 2024 4th International Conference on AI and Signal Processing (AISP), Vijayawada, India, 2024, pp. 1–5, doi: 10.1109/AISP61711.2024.10870623.

[5] T. A. Elwi, Z. A. Rhazali, H. Misran, M. M. Ismael, and B. B. Q. Elias, "A Beam-Split and Gain-Enhanced Patch Antenna Using Metamaterial Superstrate for Wireless Communications," Informacije MIDEM, vol. 55, no. 3, 2025.

[6] M. N. N. Alaukally, M. Ilyas, and T. A. Oleiwi, "On the performance revision of a wearable antenna sensor for glucose detection utilizing artificial neural networks," Power System Technology, vol. 49, no. 2, pp. 1121–1155, May 2025.

[7] T. Tong, Y. Chen, Z. Deng, and E. Hu, "An Off-Grid DOA Estimation Method via Fast Variational Sparse Bayesian Learning," Electronics, vol. 14, 2025, Art. no. 2781. doi: 10.3390/electronics14142781.

[8] S. Burchfield, C. Givhan, and S. Martin, "A Beam Steering Vector Tracking GNSS Software-Defined Receiver for Robust Positioning," Sensors, vol. 25, 2025, Art. no. 1951. doi: 10.3390/s25061951.

[9] Y. Al Naiemy, A. N. Abdulateef, A. R. Hamad, M. S. Ismael, B. Ruthramurthy, T. A. Elwi, L. Nagy, and T. Zwick, "A Further Realization of Binary Genetic Algorithm to Design a Dual Frequency Band Rectenna for Energy Harvesting in 5G Networks," DJES, vol. 18, no. 2, pp. 203–214, Jun. 2025.

[10] R. Adel Kamil, S. M. B. Alsabti, R. K. Abdulsattar, A. H. Mohammed, and T. A. Elwi, "On the Enhancement Anomaly Detection for RF Bio-Sensors by Computing Artificial Networks Using ML Techniques," Infocommunications Journal, vol. XVII, no. 2, pp. 89–95, Jun. 2025. doi: 10.36244/ICJ.2025.2.11.

[11] F. Taher, "Novel Reconfigurable Fractal Antenna Design for Modern Communication Systems," Journal of Advanced Research in Applied Sciences and Engineering Technology, vol. 64, no. 4, pp. 47–57, Mar. 2025.

[12] M. Mahdi Ali, E. Márquez Segura, and T. A. Elwi, "Advancements in Ku Band Resonator Composite Right/Left-Handed (CRLH) MTMs: Design, Analysis, and Applications," Journal of Engineering and Sustainable Development, vol. 29, no. 2, pp. 184–189, Mar. 2025, doi: 10.31272/jeasd.2646.

[13] Z. J. Abdulkareem, T. K. Hamad, and T. A. Elwi, "Reconfigurable metasurface based on graphene optical antennae for dynamic beam steering," Sustainable Engineering and Innovation, vol. 7, no. 1, pp. 127–136, Mar. 2025.

[14] M. H. Jwair, T. A. Elwi, S. K. Khamas, A. Farajidavar, and A. B. Ismail, "Circularly shaped metamaterial fractal reconfigurable antenna for 5G networks," International Journal of Information and Communication Technology, vol. 6, no. 3, pp. 65–75, Dec. 2023, doi: 10.31987/ijict.6.3.251.

[15] M. H. Jwair, T. A. Elwi, et al., "Intelligent metasurface layer for direct antenna amplitude modulation scheme," IEEE Access, vol. 11, pp. 77506–77517, 2023.

[16] A. Abood, H. Wang, B. S. Virdee, D. He, M. Fathy, A. A. Yusuf, O. Jamal, T. A. Elwi, M. Alibakhshikenari, L. Kouhalvandi, and A. Ahmad, "Improved 5G network slicing for enhanced QoS against attack in SDN environment using deep learning," IET Communications, vol. 18, pp. 759–777, 2024. doi: 10.1049/cmu2.12735.

[17] M. Nabeel, K. Singh, M. U. Afzal, D. N. Thalakotuna, and K. P. Esselle, "Dual-Band Passive Beam Steering Antenna Technologies for Satellite Communication and Modern Wireless Systems: A Review," Sensors, vol. 24, 2024, Art. no. 6144. doi: 10.3390/s24186144.

[18] S. Verho and J.-Y. Chung, "Design of a Compact and Minimalistic Intermediate Phase Shifting Feed Network for Ka-Band Electrical Beam Steering," Sensors, vol. 24, 2024, Art. no. 1235. doi: 10.3390/s24041235.

[19] S. Verho, V. T. Nguyen, and J.-Y. Chung, "A 4 × 4 Active Antenna Array with Adjustable Beam Steering," Sensors, vol. 23, 2023, Art. no. 1324. doi: 10.3390/s23031324.

[20] H. Hussein, T. A. Elwi, et al., "A Novel MIMO Antenna Integrated With a Solar Panel and Employing AI-Equalization for 5G Wireless Communication Networks," IEEE Access, vol. 12, pp. 114382–114393, 2024, doi: 10.1109/ACCESS.2024.3441830.

[21] M. S. Abdulrazzaq and A. A. Hameed, "Hybrid multiple access techniques performance analysis of dynamic resource allocation," International Journal of Information and Communication Technology (IJICT), vol. 7, no. 1, pp. 1–9, 2024. [Online]. Available: https://ijict.edu.iq/index.php/ijict/article/view/243. Accessed: 11-Sep-2025.

[22] Z. Attrah, M. T. Al-Sharify, A. F. Al-Janabi, G. Oğuçu Yetkın, T. A. Oleiwi, and H. H. Al-Khaylani, "Wideband MIMO 5G Antennae for Handset Devices," 2024 4th International Conference on AI and Signal Processing (AISP), Vijayawada, India, 2024, pp. 1–5, doi: 10.1109/AISP61711.2024.10870727.

[23] R. T. Salman and N. A. Kareem, "A cooperative communication system with P-LDPC for Internet of Underwater Things," International Journal of Information and Communication Technology (IJICT), vol. 7, no. 1, pp. 80–88, 2024. [Online]. Available: https://ijict.edu.iq/index.php/ijict/article/view/281. Accessed: 11-Sep-2025.

[24] A. H. Al-Bahadili and S. K. Saeed, "Secure index with OFDM-IM-based chaotic system," International Journal of Information and Communication Technology (IJICT), vol. 6, no. 3, pp. 70–79, 2023. [Online]. Available: https://ijict.edu.iq/index.php/ijict/article/view/239. Accessed: 11-Sep-2025.

[25] R. M. Zaal, N. N. Kamal, M. A. Ahmed, S. H. Ghadeer Al–Sultani, S. K. Bin and T. A. Oleiwi, "Direct Antenna Beam Squint Correction Using AI-Equalization Strategy for 3D MIMO Array System," Proceedings of the 2024 4th International Conference on AI and Signal Processing (AISP), 2024, doi: 10.1109/AISP61711.2024.10870623.

[26] J. W. Wu and R. Zhang, "Toward smart and reconfigurable environment: intelligent reflecting surface aided wireless network," IEEE Communications Magazine, vol. 58, no. 1, pp. 106–112, Jan. 2020, doi: 10.1109/MCOM.001.1900107.

[27] M. Di Renzo, M. Debbah, D. T. Phan-Huy, et al., "Smart radio environments empowered by reconfigurable AI meta-surfaces: an idea whose time has come," Journal of Wireless Communications and Networking, vol. 2019, Art. no. 129, 2019. doi: 10.1186/s13638-019-1438-9.

[28] E. Björnson, "Ö. Özdogan, and E. G. Larsson, "Intelligent Reflecting Surface Versus Decode-and-Forward: How Large Surfaces are Needed to Beat Relaying?," IEEE Wireless Communications Letters, vol. 9, no. 2, pp. 244–248, Feb. 2020, doi: 10.1109/LWC.2019.2950624.

[29] W. Tang, J.-Y. Dai, M. Chen, X. Li, Q. Cheng, S. Jin, K.-K. Wong, and T. J. Cui, "Programmable metasurface-based RF chain-free 8PSK wireless transmitter," Electronics Letters, vol. 55, pp. 417–420, 2019. doi: 10.1049/el.2019.0400.

[30] C. Huang, G. C. Alexandropoulos, C. Yuen, and M. Debbah, "Indoor Signal Focusing with Deep Learning Designed Reconfigurable Intelligent Surfaces," in 2019 IEEE 20th International Workshop on Signal Processing Advances in Wireless Communications (SPAWC), Cannes, France, 2019, pp. 1–5, doi: 10.1109/SPAWC.2019.8815412.

[31] W. Tang, Y. Jin, et al., "Wireless Communications with Programmable Metasurface: New Paradigms, Opportunities, and Challenges on Transceiver Design," IEEE Wireless

Communications, vol. 27, no. 2, pp. 180–187, Apr. 2020, doi: 10.1109/MWC.001.1900308.

[32] X. You, C. X. Wang, J. Huang, et al., "Towards 6G wireless communication networks: vision, enabling technologies, and new paradigm shifts," Science China Information Sciences, vol. 64, 2021, Art. no. 110301. doi: 10.1007/s11432-020-2955-6.

[33] L. Dai, K. -H. A. et al., "Reconfigurable Intelligent Surface-Based Wireless Communications: Antenna Design, Prototyping, and Experimental Results," IEEE Access, vol. 8, pp. 45913–45923, 2020, doi: 10.1109/ACCESS.2020.2977772.

[34] Q. Wu and R. Zhang, "Toward smart and reconfigurable environment: intelligent reflecting surface aided wireless network," IEEE Communications Magazine, vol. 58, no. 1, pp. 106–112, Jan. 2020, doi: 10.1109/MCOM.001.1900107.

[35] J. Chen, Y.-C. Liang, Y. Pei, and H. Guo, "Intelligent Reflecting Surface: A Programmable Wireless Environment for Physical Layer Security," IEEE Access, vol. 7, pp. 82599–82612, 2019, doi: 10.1109/ACCESS.2019.2924034.

[36] C. Han, L. Yan, and J. Yuan, "Hybrid Beamforming for Terahertz Wireless Communications: Challenges, Architectures, and Open Problems," IEEE Communications Magazine, 2021. [Online]. Available: [PDF].

[37] M. Giordani, M. Polese, A. Roy, D. Castor, et al., "Standalone and Non-Standalone Beam Management for 3GPP NR at mmWaves," 2018. [Online]. Available: [PDF].

[38] S. Hamid, S. R. Chopra, A. Gupta, S. Tanwar, et al., "Hybrid Beamforming in Massive MIMO for Next-Generation Communication Technology," 2023. [Online]. Available: ncbi.nlm.nih.gov.

[39] S. Subramanyam Thoota, J. Vieira, and E. G. Larsson, "Data-Driven Robust Beamforming for Initial Access," 2023. [Online]. Available: [PDF].

[40] T. Zheng, J. Zhu, Q. Yu, and Y. Yan, "Coded Beam Training," 2024. [Online]. Available: [PDF].

[41] K. Bechta, C. Ziółkowski, J. M. Kelner, and L. Nowosielski, "Modeling of Downlink Interference in Massive MIMO 5G Macro-Cell," 2021. [Online]. Available: ncbi.nlm.nih.gov.

[42] S. Khosravi, H. S. Ghadikolaeiy, J. Zander, and M. Petrova, "Location-Aided Beamforming in Mobile Millimeter-Wave Networks," 2022. [Online]. Available: [PDF].

[43] X. Xu, Y. Liu, X. Mu, Q. Chen, et al., "AI Enabled NOMA Towards Next Generation Multiple Access," 2022. [Online]. Available: [PDF].

[44] M. Asif, A. Ihsan, W. Ullah Khan, and A. Ranjha, "Energy-Efficient Beamforming and Resource Optimization for AmBSC-Assisted Cooperative NOMA IoT Networks," 2022. [Online]. Available: [PDF].

[45] S. Agha Hassnain Mohsan and Y. Li, "A Survey of NOMA: State of the Art, Key Techniques, Open Challenges, Security Issues and Future Trends," 2023. [Online]. Available: [PDF].

[46] Z. Ding and H. V. Poor, "On the Application of BAC-NOMA to 6G umMTC," 2021. [Online]. Available: [PDF].

[47] Y. Liu, S. Zhang, X. Mu, Z. Ding, et al., "Evolution of NOMA Toward Next Generation Multiple Access (NGMA) for 6G," 2021. [Online]. Available: [PDF].

[48] S. M. R. Islam, M. Zeng, O. A. Dobre, and K. S. Kwak, "NOMA: How It Meets 5G and Beyond," 2019. [Online]. Available: [PDF].

[49] Z. Ding, X. Lei, G. K. Karagiannidis, R. Schober, et al., "A Survey on Non-Orthogonal Multiple Access for 5G Networks: Research Challenges and Future Trends," IEEE Communications Surveys & Tutorials, 2017. [Online]. Available: [PDF].

[50] S. Zeb, Q. Abbas, S. A. Hassan, and A. Mahmood, "NOMA Enhanced Backscatter Communication for Green IoT Networks," 2019. [Online]. Available: [PDF].

[51] J. Li, C. Wan Sung, and C. Shue Chen, "Performance Study of Cooperative Non-Orthogonal Multiple Access with Energy Harvesting," 2019. [Online]. Available: [PDF].

[52] J. Shi, W. Yu, Q. Ni, and W. Liang, "Energy Efficient Resource Allocation in Hybrid Non-Orthogonal Multiple Access Systems," 2019. [Online]. Available: [PDF].

[53] O. Habachi, M. A. Adjif, and J. P. Cances, "Fast Uplink Grant for NOMA: a Federated Learning based Approach," 2019. [Online]. Available: [PDF].

[54] S. Rajkumar and D. Nalin K. Jayakody, "Backscatter Assisted NOMA-PLNC Based Wireless Networks," 2021. [Online]. Available: ncbi.nlm.nih.gov.

[55] Y. Tian, G. Pan, and M.-S. Alouini, "On NOMA-Based mmWave Communications," 2020. [Online]. Available: [PDF].

[56] Z. Lin, S. Cao, and J. Li, "Time Switching Based Wireless Powered Relay Transmission with Uplink NOMA," 2021. [Online]. Available: ncbi.nlm.nih.gov.

[57] A. Magbool, H. Sarieddeen, N. Kouzayha, M.-S. Alouini, et al., "Terahertz-Band Non-Orthogonal Multiple Access: System- and Link-Level Considerations," 2021. [Online]. Available: [PDF].

[58] S. Govindasamy, D. W. Bliss, and D. H. Staelin, "Asymptotic Spectral Efficiency of the Uplink in Spatially Distributed Wireless Networks With Multi-Antenna Base Stations," 2011. [Online]. Available: [PDF].

[59] D. Wang, Y. Zhang, H. Wei, and X. You, "An Overview of Transmission Theory and Techniques of Large-scale Antenna Systems for 5G Wireless Communications," 2016. [Online]. Available: [PDF].

[60] J. Lota, S. Sun, T. S. Rappaport, A. Demosthenous, et al., "5G Uniform linear arrays with beamforming and spatial multiplexing at 28 GHz, 37 GHz, 64 GHz and 71 GHz for outdoor urban communication: A two-level approach," 2017. [Online]. Available: [PDF].

[61] C. Han, L. Yan, and J. Yuan, "Hybrid Beamforming for Terahertz Wireless Communications: Challenges, Architectures, and Open Problems," 2021. [Online]. Available: [PDF].

[62] J. Zhang, X. Yu, and K. B. Letaief, "Hybrid Beamforming for 5G and Beyond Millimeter-Wave Systems: A Holistic View," 2019. [Online]. Available: [PDF].